

Mode interaction in external flows

Competing fluid instabilities in wake and jet flows.

Javier Sierra-Ausin^{1,2}

Supervised by: Flavio Giannetti¹ and David Fabre²

¹ UNISA-DIIN, Università degli Studi di Salerno, Fisciano 84084, Italy

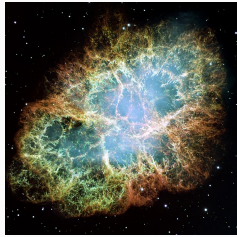
² UPS-IMFT, Institut de Mécanique des fluides de Toulouse, CNRS, Toulouse 31400, France



UNIVERSITÀ DEGLI STUDI
DI SALERNO

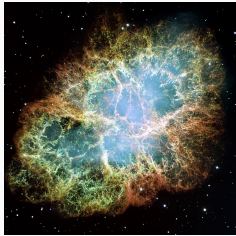
Fluid dynamic instabilities in nature

Rayleigh-Taylor – Crab Nebula

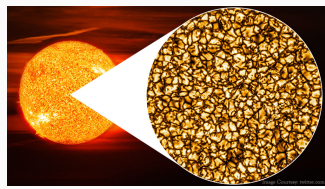


Fluid dynamic instabilities in nature

Rayleigh-Taylor – Crab Nebula

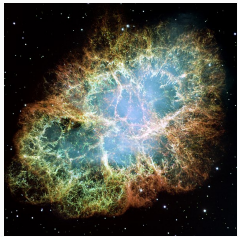


Rayleigh-Benard– Sun surface



Fluid dynamic instabilities in nature

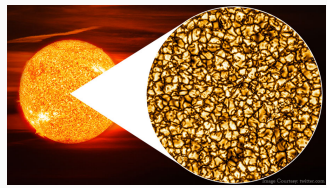
Rayleigh-Taylor – Crab Nebula



Kelvin-Helmholtz – Clouds of Jupiter

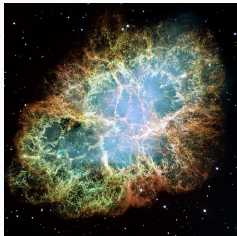


Rayleigh-Benard – Sun surface



Fluid dynamic instabilities in nature

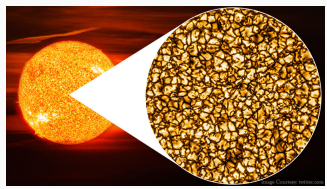
Rayleigh-Taylor – Crab Nebula



Kelvin-Helmholtz – Clouds of Jupiter



Rayleigh-Benard – Sun surface

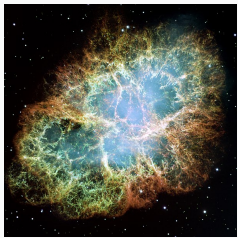


Crow – Condensation trail



Fluid dynamic instabilities in nature

Rayleigh-Taylor – Crab Nebula



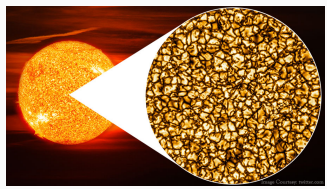
Kelvin-Helmholtz – Clouds of Jupiter



Rayleigh-Plateau – Rain water dripping



Rayleigh-Benard – Sun surface

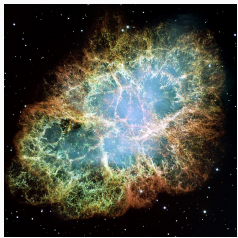


Crow – Condensation trail



Fluid dynamic instabilities in nature

Rayleigh-Taylor – Crab Nebula



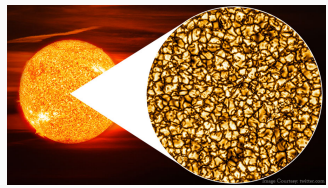
Kelvin-Helmholtz – Clouds of Jupiter



Rayleigh-Plateau – Rain water dripping



Rayleigh-Benard – Sun surface



Crow – Condensation trail

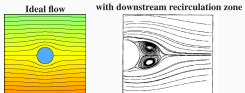


Marangoni – Tears of wine



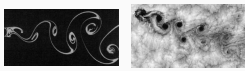
Fluid dynamic instabilities in nature

Vortex shedding



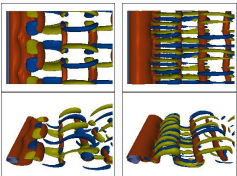
First transition

Von Kármán vortex street ($Re \geq 46$)



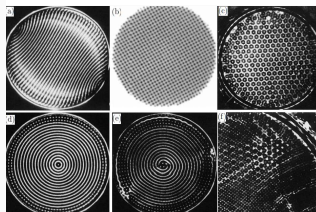
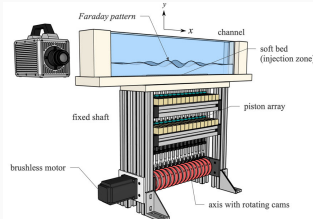
3D transition

mode A at $Re = 210$ mode B at $Re = 250$



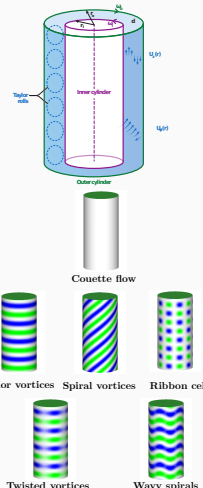
Extracted from:
[1] Thompson et al.
[2] L. Tuckermann, Lecture Notes in Nonlinear Dynamics

Faraday waves



Extracted from:
[1] Orphee et al.
[2] Juan F. Marín et al.

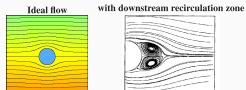
Taylor–Couette



Top figure extracted from:
[1] Grossmann. Annual Review in Fluid Mechanics

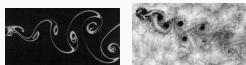
Bifurcations – A matter of breaking spatio-temporal symmetries

Vortex shedding



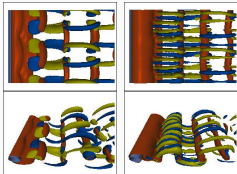
First transition

Von Kármán vortex street ($Re \geq 46$)



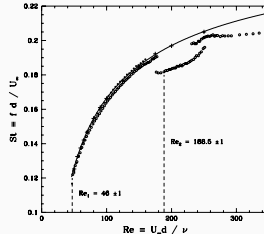
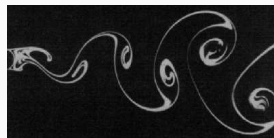
3D transition

mode A at $Re = 210$ mode B at $Re = 250$



Extracted from:
[1] Thompson et al.
[2] L. Tuckermann, Lecture Notes in Nonlinear Dynamics

Spatio-temporal symmetries: first transition



Spatio-temporal symmetric

$$U(x, y, z, t) = U(x, -y, z, t + T/2),$$

$$V(x, y, z, t) = -V(x, -y, z, t + T/2)$$

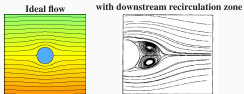
A game of breaking symmetries

Reflectional symmetry after half-period

Homogeneous in z

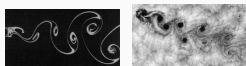
Bifurcations – A matter of breaking spatio-temporal symmetries

Vortex shedding



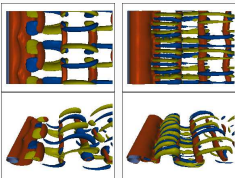
First transition

Von Kármán vortex street ($Re \geq 46$)



3D transition

mode A at $Re = 210$ mode B at $Re = 250$



Extracted from:

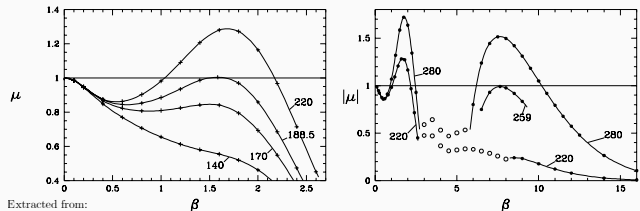
[1] Thompson et al.

[2] L. Tuckermann, Lecture Notes in Nonlinear Dynamics

Break of the homogeneous symmetry in z

$$\mathbf{u}(x, y, z, t) = \mathbf{u}_{2D} + \mathbf{u}'_{3D}(x, y, z, t) \text{ with}$$

$$\mathbf{u}'_{3D}(x, y, z, t) = e^{i\beta_c z} e^{\lambda_\beta t} \hat{\mathbf{u}}_\beta(x, y, t \bmod T)$$



Extracted from:

[1] Barkley & Henderson, J. Fluid Mech. (1996).

[2] L. Tuckermann, Lecture Notes in Nonlinear Dynamics

Mode A

$$Re_c = 188.5, \beta_c = 1.585$$

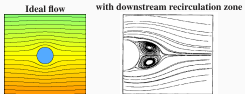
Temporally: Steady bifurcation ($\lambda_\beta \in \mathbb{R}$) Spatially: Pitchfork of revolution (arbitrary phase in z)

Mode B

$$Re_c = 259, \beta_c = 7.64$$

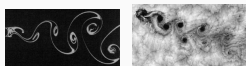
Bifurcations – A matter of breaking spatio-temporal symmetries

Vortex shedding



First transition

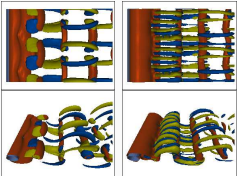
Von Kármán vortex street ($Re \geq 46$)



Laboratory experiment
(Taneda, 1982) Off Chilean coast
past Juan Fernandez islands

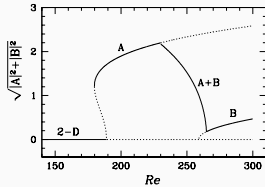
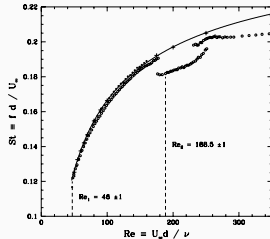
3D transition

mode A at $Re = 210$ mode B at $Re = 250$



Extracted from:
[1] Thompson et al.
[2] L. Tuckermann, Lecture Notes in Nonlinear Dynamics

A first example of mode interaction



Extracted from:

- [1] Barkley, Tuckerman & Golubitsky, PRE (2000)
- [2] L. Tuckermann, Lecture Notes in Nonlinear Dynamics

A model for the **jump** transition between Mode A and B

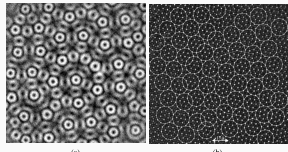
$$A_{n+1} = (\mu_A A_n + \alpha_A |A_n|^2 + \gamma_A |B_n|^2 - \beta_A |A_n|^4) A_n$$

$$B_{n+1} = (\mu_B B_n + \alpha_B |B_n|^2 + \gamma_B |B_n|^2) B_n$$

Spatio-temporal symmetries – Quasipatterns in the Faraday experiment

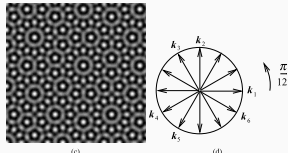
Quasipatterns in a lattice

These serve as an example of
"local" symmetries.



(a)

(b)



(c)

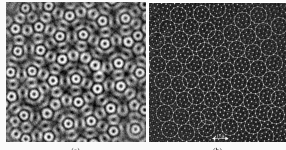
(d)

$$u(x) = \sum_{n=1}^6 A_n e^{ik_n \cdot x} + \text{c.c.}$$

Spatio-temporal symmetries – Quasipatterns in the Faraday experiment

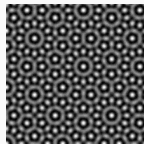
Quasipatterns in a lattice

These serve as an example of "local" symmetries.

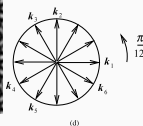


(a)

(b)



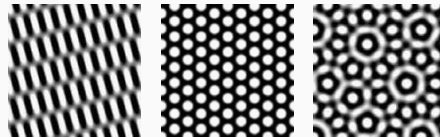
(c)



(d)

$$u(x) = \sum_{n=1}^6 A_n e^{ik_n \cdot x} + \text{c.c.}$$

How can we break the dodecagonal lattice?



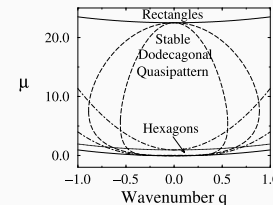
Rectangles

$$\partial_t A_i = \mu A_i + (\hat{\mathbf{n}}_i \cdot \hat{\nabla})^2 A_i + \alpha \overline{A_{i+2} A_{i+4}} - A_i (|A_i|^2 + \nu(|A_{i+2}|^2 + |A_{i+4}|^2)) + \gamma(|A_{i-1}|^2 + |A_{i-3}|^2) + 2\beta|A_{i+1}|^2, \quad i = 1, 3, 5,$$

$$\partial_t A_i = \mu A_i + (\hat{\mathbf{n}}_i \cdot \hat{\nabla})^2 A_i + \alpha \overline{A_{i+2} A_{i+4}} - A_i (|A_i|^2 + \nu(|A_{i+2}|^2 + |A_{i+4}|^2)) + \gamma(|A_{i+1}|^2 + |A_{i+3}|^2) + 2\beta|A_{i-1}|^2, \quad i = 2, 4, 6.$$

Hexagons

Dodecagons

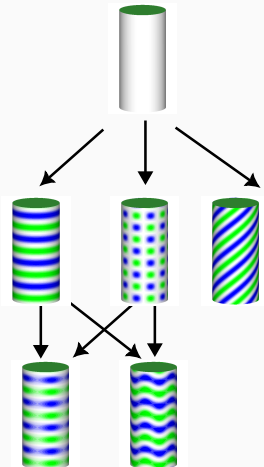


$$\alpha = 1 \text{ and } \nu = 0.7, \gamma = 0.3 \text{ and } \beta = 0.5$$

Extracted from Echeberria and Riecke (2001)

Bifurcations – A matter of breaking spatio-temporal symmetries

Classification



A kind of interaction in Taylor-Couette

Equivariant under the group $O(2) \times S^1 \times SO(2)$

Taylor vortex: Break of z -invariance.

Spirals: Rotating waves travelling in the z -direction.

Ribbons: Standing Waves

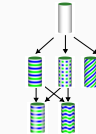
$$\begin{aligned} q(t, \tau) = & Q_0 + \operatorname{Re}(a_0(\tau)e^{-i\beta_0 z}\hat{q}_0) \\ & + \operatorname{Re}(a_1(\tau)e^{-i\omega t}e^{-i\beta_1 z}\hat{q}_1) \\ & + \operatorname{Re}(a_2(\tau)e^{-i\omega t}e^{i\beta_1 z}\hat{q}_2) \end{aligned}$$

$$\begin{aligned} \dot{a}_0 = & \lambda_s a_0 + l_0 a_0 |a_0|^2 + l_1 (|a_1|^2 + |a_2|^2) a_0 \\ & + i l_2 (|a_2|^2 - |a_1|^2) a_0 + l_3 \bar{a}_0 \bar{a}_2 a_1 \end{aligned}$$

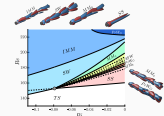
$$\begin{aligned} \dot{a}_1 = & (\lambda_h + i\omega_h) a_1 + (B|a_1|^2 + (A+B)|a_2|^2) a_1 \\ & + C a_1 |a_0|^2 + D a_0^2 a_2 \end{aligned}$$

$$\begin{aligned} \dot{a}_2 = & (\lambda_h + i\omega_h) a_2 + (B|a_2|^2 + (A+B)|a_1|^2) a_2 \\ & + C a_2 |a_0|^2 + D \bar{a}_0^2 a_1 \end{aligned}$$

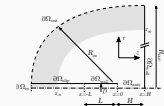
Outline of research works



Slow-fast dynamics of the wake behind bluff bodies



Dynamics of a rounded laminar impinging jet



Conclusion

Outline of the thesis – Mode interactions in external flows

Mode interaction

1. J. Sierra, V. Citro, D. Fabre, F. Giannetti. Bifurcation scenario in the two-dimensional laminar flow past a rotating cylinder. *JFM* 905.
2. J. Sierra, M. Lorite, J.I. Jimenez, V. Citro, D. Fabre. Unveiling the competitive role of global modes in the pattern formation of rotating sphere flows. *JFM* 942.
3. J. Sierra, D. Fabre, E. Knobloch. A Note on the steady-state mode and Hopf mode interaction in the presence of $O(2)$ -symmetry. *PRE (submitted)*
4. A. Corrochano, J. Sierra, J.A. Martin, S. Le Clainche, D. Fabre. Mode selection in concentric jets with resonance 1:2 *JFM (under review)*
5. J. Sierra, F. Giannetti, D. Fabre, P. Luchini. On the linear and nonlinear mechanisms for the tonal and broadband noise of subsonic rounded impinging jet *JFM (submitted)*

Linear stability of problems with moving interfaces

1. J. Sierra, P. Bonnefis, A. Tirri, D. Fabre, J. Magnaudet. Dynamics of a gas bubble in a straining flow: deformation, oscillations, self-propulsion. *PRF*, 7(11), 113603.
2. A. Tirri, A. Nitti, J. Sierra, F. Giannetti, M. D. de Tullio. Linear stability analysis of fluid–structure interaction problems with an immersed boundary method. *JFS*, 117.

Applications in acoustics/compressible flows

1. J. Sierra, V. Citro, D. Fabre, F. Giannetti. Acoustic instability prediction of the flow through a circular aperture in a thick plate via an impedance criterion. *JFM 943*.
2. L. Hirschberg, J. I. Guzman, A. Morgans, J. Sierra, D. Fabre, A. Hirschberg. Linear Theory and Experiments for Laminar Bias Flow Impedance. *AIAA to be submitted*.

Applications in acoustics/compressible flows

1. J. Sierra, V. Citro, D. Fabre, F. Giannetti. Acoustic instability prediction of the flow through a circular aperture in a thick plate via an impedance criterion. *JFM* 943.
2. L. Hirschberg, J. I. Guzman, A. Morgans, J. Sierra, D. Fabre, A. Hirschberg. Linear Theory and Experiments for Laminar Bias Flow Impedance. *AIAA to be submitted*.

Numerical methods

1. J. Sierra, P. Jolivet, V. Citro, F. Giannetti. Adjoint-based sensitivity analysis of periodic orbits by the Fourier–Galerkin method *JCP* 440
2. J. Sierra, V. Citro, D. Fabre, F. Giannetti. Efficient computation of time-periodic compressible flows with spectral techniques *CMAME* 393.
3. J. Sierra, V. Citro, D. Fabre. Efficient stability analysis of fluid flows using complex mapping techniques. *CPC* 251.

Applications in acoustics/compressible flows

1. J. Sierra, V. Citro, D. Fabre, F. Giannetti. Acoustic instability prediction of the flow through a circular aperture in a thick plate via an impedance criterion. *JFM* 943.
2. L. Hirschberg, J. I. Guzman, A. Morgans, J. Sierra, D. Fabre, A. Hirschberg. Linear Theory and Experiments for Laminar Bias Flow Impedance. *AIAA to be submitted*.

Numerical methods

1. J. Sierra, P. Jolivet, V. Citro, F. Giannetti. Adjoint-based sensitivity analysis of periodic orbits by the Fourier–Galerkin method *JCP* 440
2. J. Sierra, V. Citro, D. Fabre, F. Giannetti. Efficient computation of time-periodic compressible flows with spectral techniques *CMAME* 393.
3. J. Sierra, V. Citro, D. Fabre. Efficient stability analysis of fluid flows using complex mapping techniques. *CPC* 251.

Outline of the thesis – Mode interactions in external flows

Applications in acoustics/compressible flows

1. J. Sierra, V. Citro, D. Fabre, F. Giannetti. Acoustic instability prediction of the flow through a circular aperture in a thick plate via an impedance criterion. *JFM* 943.
2. L. Hirschberg, J. I. Guzman, A. Morgans, J. Sierra, D. Fabre, A. Hirschberg. Linear Theory and Experiments for Laminar Bias Flow Impedance. *AIAA to be submitted*.

Numerical methods

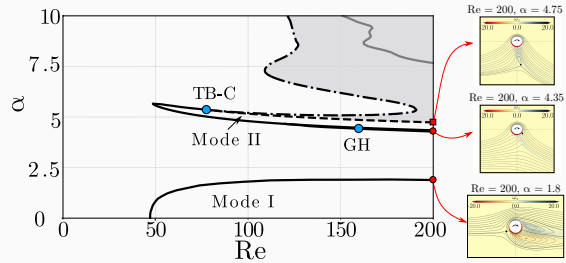
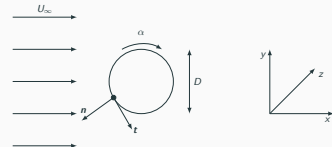
1. J. Sierra, P. Jolivet, V. Citro, F. Giannetti. Adjoint-based sensitivity analysis of periodic orbits by the Fourier–Galerkin method *JCP* 440
2. J. Sierra, V. Citro, D. Fabre, F. Giannetti. Efficient computation of time-periodic compressible flows with spectral techniques *CMAME* 393.
3. J. Sierra, V. Citro, D. Fabre. Efficient stability analysis of fluid flows using complex mapping techniques. *CPC* 251.

Miscellaneous

- a. J. Sierra, V. Citro, F. Giannetti. Optimal explicit Runge-Kutta methods for compressible Navier-Stokes equations. *ANM*.
- b. G. Saez, J. Sierra, J. Gressier. Spectral Difference Raviart–Thomas Method for Two and Three-Dimensional Elements and Its Connection with the Flux Reconstruction Formulation. *JSciComp*.
- c. G. Saez, J. Sierra, G. Grondin, J. Gressier. On the properties of high-order least-squares finite-volume schemes. *JCP*

Mode interaction – Takens-Bogdanov – Spinning cylinder

Sierra Javier et al. (2020). Bifurcation scenario in the two-dimensional laminar flow past a rotating cylinder.

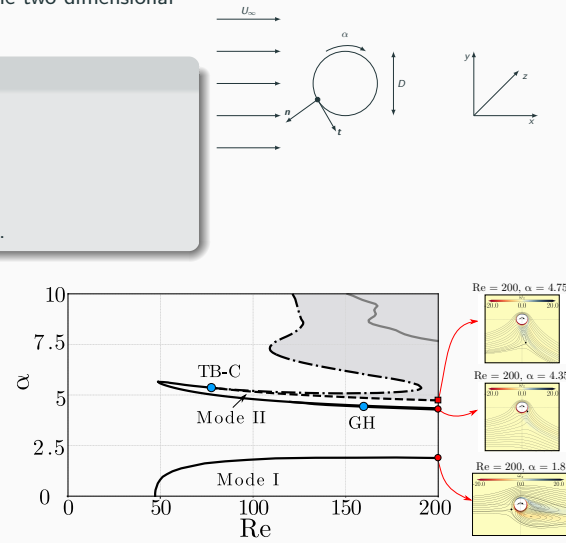
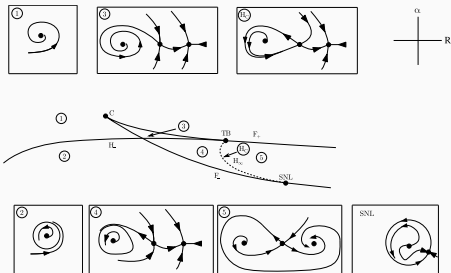


Mode interaction – Takens-Bogdanov – Spinning cylinder

Sierra Javier et al. (2020). Bifurcation scenario in the two-dimensional laminar flow past a rotating cylinder.

Organizing centre: Focus Takens-Bogdanov

- Existence of multiple steady-states:hysteresis.
- Existence of a SNIPER bifurcation.
- Birth of the unsteady Mode II branch.
- Existence of a cusp point close to the TB point.

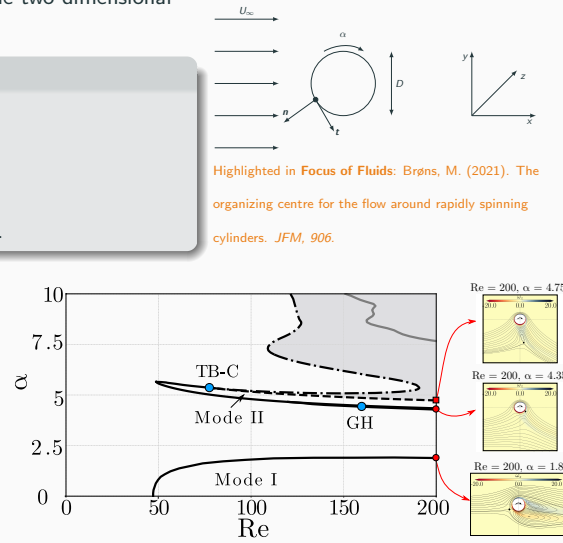
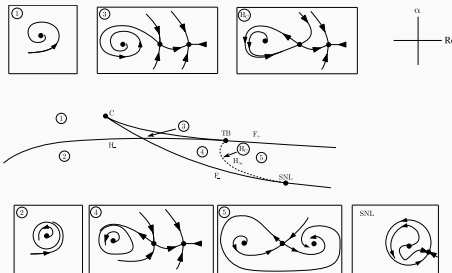


Mode interaction – Takens-Bogdanov – Spinning cylinder

Sierra Javier et al. (2020). Bifurcation scenario in the two-dimensional laminar flow past a rotating cylinder.

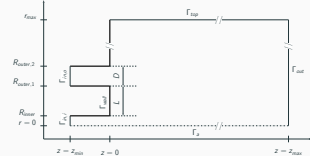
Organizing centre: Focus Takens-Bogdanov

- Existence of multiple steady-states:hysteresis.
- Existence of a SNIPER bifurcation.
- Birth of the unsteady Mode II branch.
- Existence of a cusp point close to the TB point.



Mode interaction – Steady-steady 1:2 – Coaxial jets

Corrochano et al. (2020). Mode selection in concentric jets with resonance 1:2. (under review for JFM)

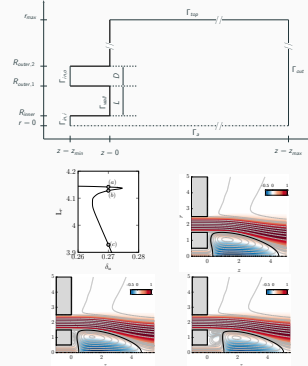


Mode interaction – Steady-steady 1:2 – Coaxial jets

Corrochano et al. (2020). Mode selection in concentric jets with resonance 1:2. (under review for JFM)

Key take-aways

- Existence of saddle-node bifurcations. *Connected to changes in the topology of the flow.*

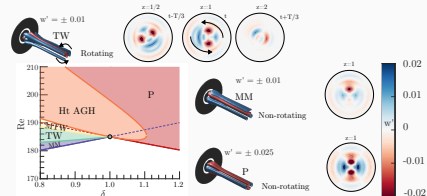
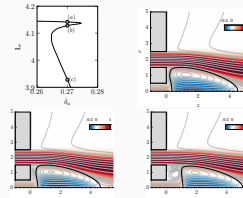
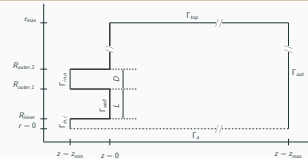


Mode interaction – Steady-steady 1:2 – Coaxial jets

Corrochano et al. (2020). Mode selection in concentric jets with resonance 1:2. (under review for JFM)

Key take-aways

- Existence of saddle-node bifurcations. *Connected to changes in the topology of the flow.*
- Existence of symmetry-breaking modes (Pure and mixed modes)

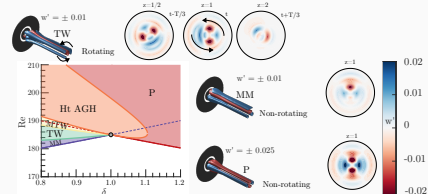
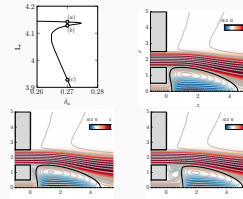
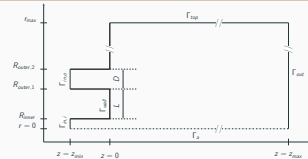


Mode interaction – Steady-steady 1:2 – Coaxial jets

Corrochano et al. (2020). Mode selection in concentric jets with resonance 1:2. (under review for JFM)

Key take-aways

- Existence of saddle-node bifurcations. *Connected to changes in the topology of the flow.*
- Existence of symmetry-breaking modes (Pure and mixed modes)
- Existence of rotating waves (TW)

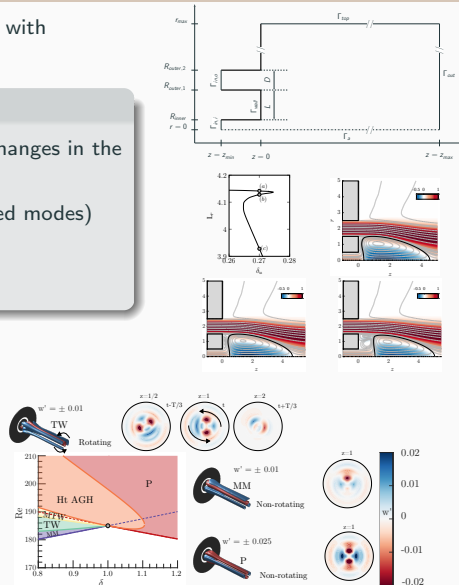
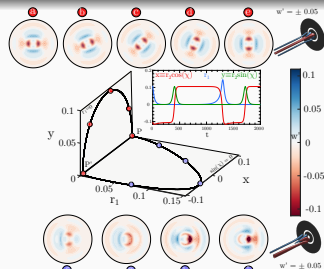


Mode interaction – Steady-steady 1:2 – Coaxial jets

Corrochano et al. (2020). Mode selection in concentric jets with resonance 1:2. (under review for JFM)

Key take-aways

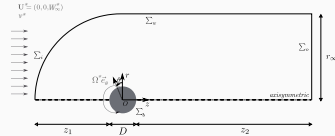
- Existence of saddle-node bifurcations. *Connected to changes in the topology of the flow.*
- Existence of symmetry-breaking modes (Pure and mixed modes)
- Existence of rotating waves (TW)
- Existence of robust heteroclinic-cycles.



Mode interaction in external flows

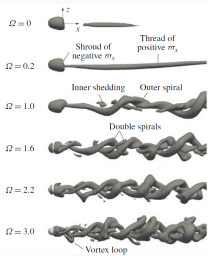
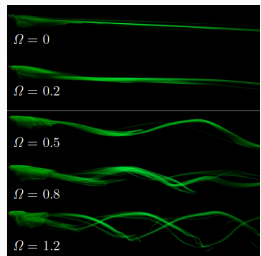
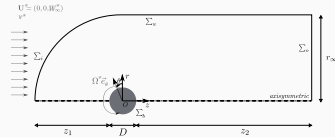
Mode interaction – Triple Hopf (non-res.) – Wake of rotating particles

J. Sierra et al. (2022). Unveiling the competitive role of global modes in the pattern formation of rotating sphere flows.



Mode interaction – Triple Hopf (non-res.) – Wake of rotating particles

J. Sierra et al. (2022). Unveiling the competitive role of global modes in the pattern formation of rotating sphere flows.



Applications

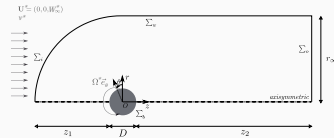
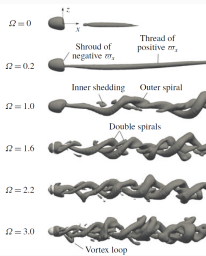
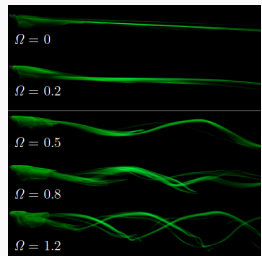
- Particle-driven flows.
- Fluidized bed combustion.
- Sport aerodynamics.
- Seeds' flight.

Mode interaction – Triple Hopf (non-res.) – Wake of rotating particles

J. Sierra et al. (2022). Unveiling the competitive role of global modes in the pattern formation of rotating sphere flows.

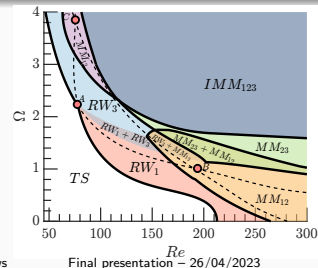
Triple Hopf (non-resonant)

- Classification of wake patterns.



Applications

- Particle-driven flows.
- Fluidized bed combustion.
- Sport aerodynamics.
- Seeds' flight.

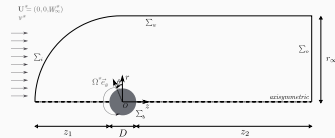
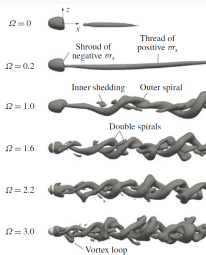
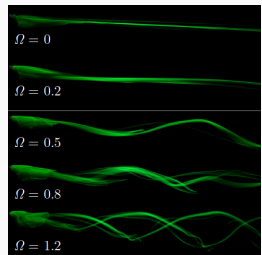


Mode interaction – Triple Hopf (non-res.) – Wake of rotating particles

J. Sierra et al. (2022). Unveiling the competitive role of global modes in the pattern formation of rotating sphere flows.

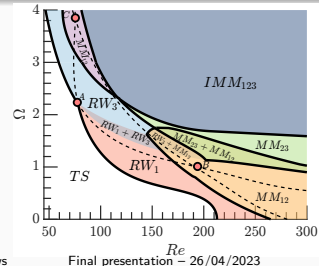
Triple Hopf (non-resonant)

- Classification of wake patterns.
- Coexistence of single and double helix patterns (RW) and (MM).



Applications

- Particle-driven flows.
- Fluidized bed combustion.
- Sport aerodynamics.
- Seeds' flight.

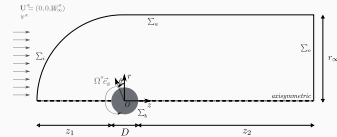
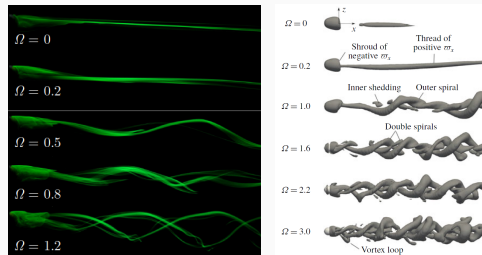


Mode interaction – Triple Hopf (non-res.) – Wake of rotating particles

J. Sierra et al. (2022). Unveiling the competitive role of global modes in the pattern formation of rotating sphere flows.

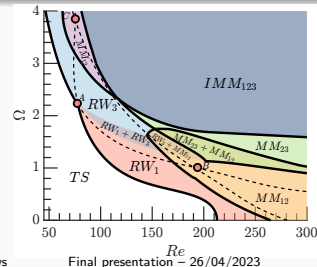
Triple Hopf (non-resonant)

- Classification of wake patterns.
- Coexistence of single and double helix patterns (RW) and (MM).
- Transition to chaos preceded by a \mathbb{T}^3 state.



Applications

- Particle-driven flows.
- Fluidized bed combustion.
- Sport aerodynamics.
- Seeds' flight.



Acoustics – Instability prediction with an impedance criterion

J. Sierra et al. (2022). Acoustic instability prediction of the flow through a circular aperture in a thick plate via an impedance criterion.

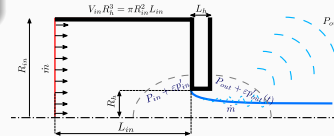
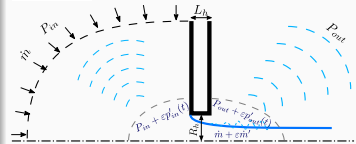


Acoustics – Instability prediction with an impedance criterion

J. Sierra et al. (2022). Acoustic instability prediction of the flow through a circular aperture in a thick plate via an impedance criterion.

Instability – Flow through a circular aperture

- Determination of the instability for the *closed* and *open* configurations.

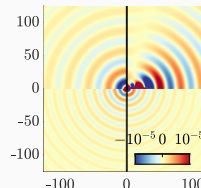
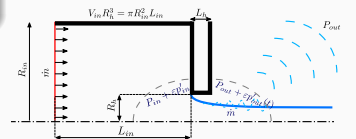
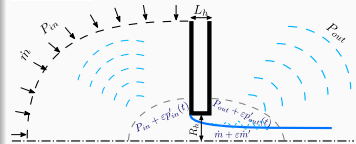


Acoustics – Instability prediction with an impedance criterion

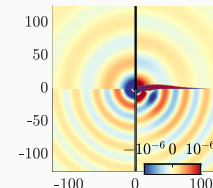
J. Sierra et al. (2022). Acoustic instability prediction of the flow through a circular aperture in a thick plate via an impedance criterion.

Instability – Flow through a circular aperture

- Determination of the instability for the *closed* and *open* configurations.
- Validation of the model against compressible LNSE.



Mode interaction in external flows



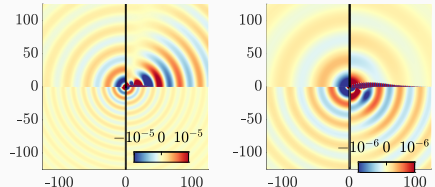
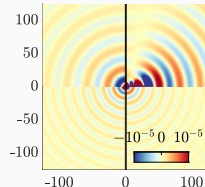
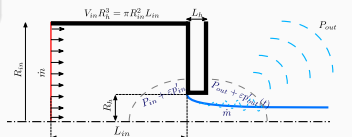
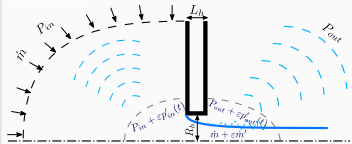
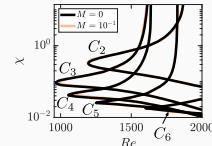
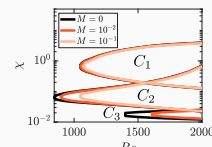
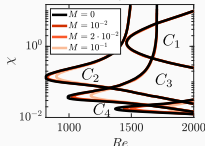
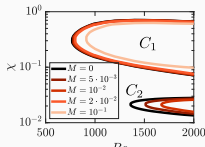
Final presentation – 26/04/2023

Acoustics – Instability prediction with an impedance criterion

J. Sierra et al. (2022). Acoustic instability prediction of the flow through a circular aperture in a thick plate via an impedance criterion.

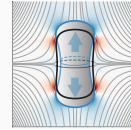
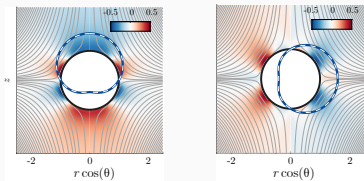
Instability – Flow through a circular aperture

- Determination of the instability for the *closed* and *open* configurations.
- Validation of the model agains compressible LNSE.
- (*Fast*) Parametric study of instability in terms of the properties of the acoustic resonator.



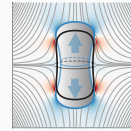
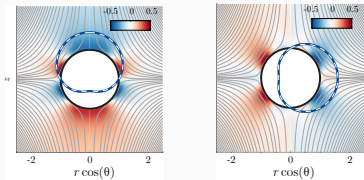
Linear stability of problems with moving interface

J. Sierra et al. (2022). Dynamics of a gas bubble in a straining flow: Deformation, oscillations, self-propulsion.



Linear stability of problems with moving interface

J. Sierra et al. (2022). Dynamics of a gas bubble in a straining flow: Deformation, oscillations, self-propulsion.



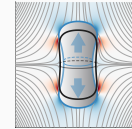
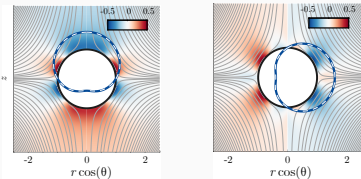
Key take-aways

Application of novel L-ALE for stability computations.

Existence of a *self-propelled* mode.

Linear stability of problems with moving interface

J. Sierra et al. (2022). Dynamics of a gas bubble in a straining flow: Deformation, oscillations, self-propulsion.

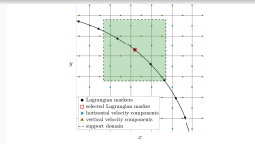
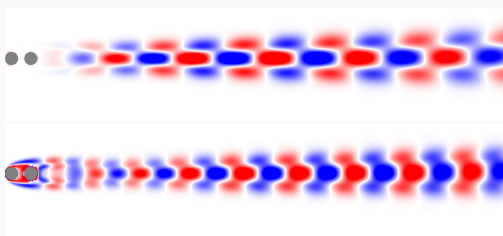


Key take-aways

Application of novel L-ALE for stability computations.

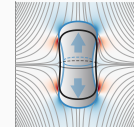
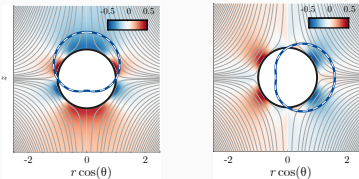
Existence of a *self-propelled* mode.

A. Tirri et al. (2023). Linear stability analysis of fluid–structure interaction problems with an immersed boundary method.



Linear stability of problems with moving interface

J. Sierra et al. (2022). Dynamics of a gas bubble in a straining flow: Deformation, oscillations, self-propulsion.

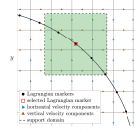
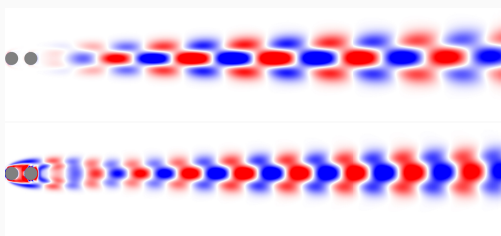


Key take-aways

Application of novel L-ALE for stability computations.

Existence of a *self-propelled* mode.

A. Tirri et al. (2023). Linear stability analysis of fluid–structure interaction problems with an immersed boundary method.



Key take-aways

Linearised IBM method for FSI problems.
Application to VIV two-cylinders configuration.

- J. Sierra et al. (2020) *Efficient stability analysis fluid flows using complex mapping techniques.*

Key take-aways

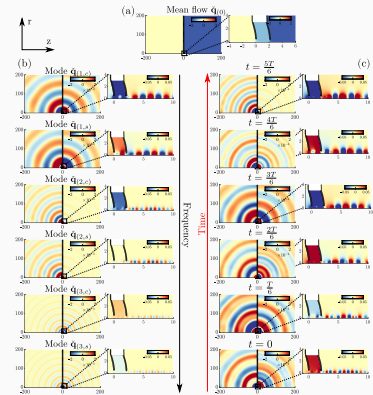
- Efficient non-reflecting boundary condition.

Numerical methods

- J. Sierra et al. (2020) *Efficient stability analysis fluid flows using complex mapping techniques.*
- J. Sierra et al. (2022) *Efficient computation of time-periodic compressible flows with spectral techniques.*

Key take-aways

- Efficient non-reflecting boundary condition.
- Computation of limit cycles for compressible.

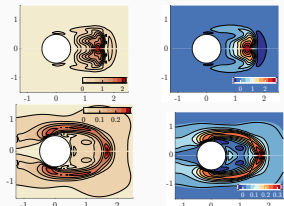


Numerical methods

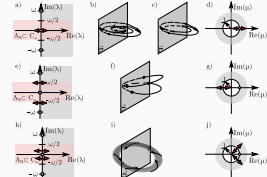
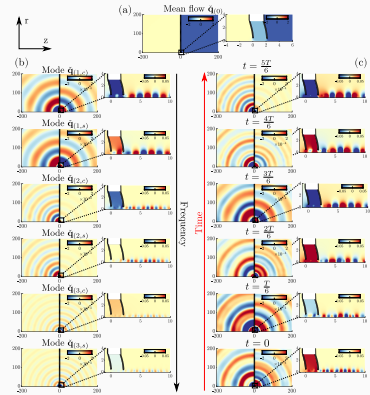
- J. Sierra et al. (2020) *Efficient stability analysis fluid flows using complex mapping techniques.*
- J. Sierra et al. (2022) *Efficient computation of time-periodic compressible flows with spectral techniques.*
- J. Sierra et al. (2021) *Adjoint-based sensitivity analysis of periodic orbits by the Fourier–Galerkin method.*

Key take-aways

- Efficient non-reflecting boundary condition.
- Computation of limit cycles for compressible.
- Floquet-Hill linear stability of the cycle.
- Sensitivity (structural/frequency var.) of L.C.



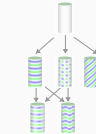
Mode interaction in external flows



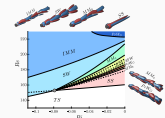
Final presentation – 26/04/2023

Outline

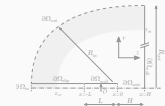
Outline of research works



Slow-fast dynamics of the wake behind bluff bodies

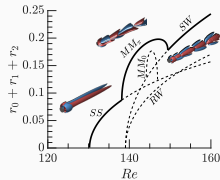


Dynamics of a rounded laminar impinging jet



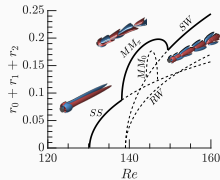
Conclusion

Wake past a fixed thin disk



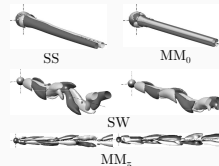
[4] Inspired from:
Meliga et al.

Wake past a fixed thin disk



[4] Inspired from:
Meliga et al.

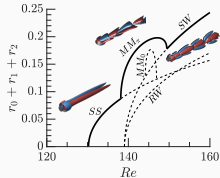
Fixed sphere in mixed-convection



Extracted from:
[3] Kotouc et al.

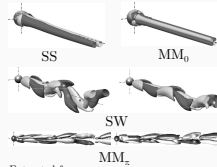
Motivation

Wake past a fixed thin disk



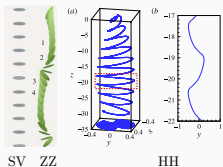
[4] Inspired from:
Meliga et al.

Fixed sphere in mixed-convection



Extracted from:
[3] Kotouc et al..

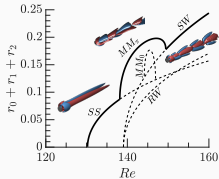
Falling object in a quiescent flow



Extracted from:
[1] Auguie et al..

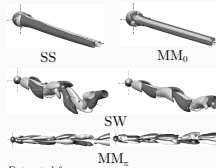
Motivation

Wake past a fixed thin disk



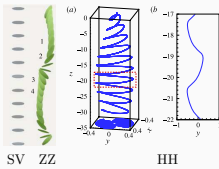
[4] Inspired from:
Meliga et al.

Fixed sphere in mixed-convection



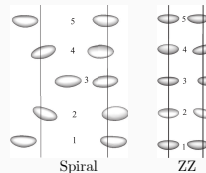
Extracted from:
[3] Kotouc et al.

Falling object in a quiescent flow



Extracted from:
[1] Auguète et al.

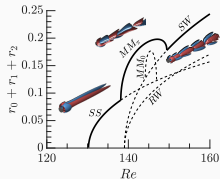
Rising bubble in a quiescent flow



Extracted from:
[2] Cano et al.

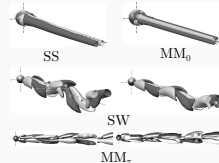
Motivation

Wake past a fixed thin disk



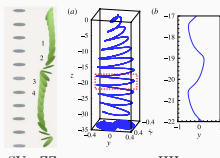
[4] Inspired from:
Meliga et al.

Fixed sphere in mixed-convection



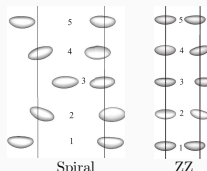
Extracted from:
[3] Kotouc et al..

Falling object in a quiescent flow



Extracted from:
[1] Auguète et al..

Rising bubble in a quiescent flow

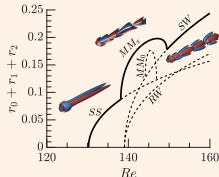


Extracted from:
[2] Cano et al..

How can we classify the distinct *coherent structures* of the flow and *trajectories* of the object?

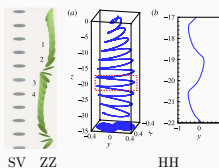
Motivation

Wake past a fixed thin disk



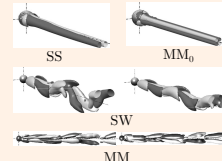
[4] Inspired from:
Meligia et al.

Falling object in a quiescent flow



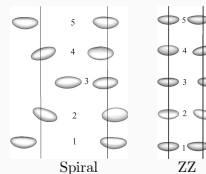
Extracted from:
[1] Auguste et al.

Fixed sphere in mixed-convection



Extracted from:
[3] Kotouc et al..

Rising bubble in a quiescent flow

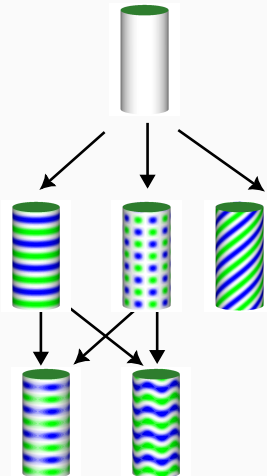


Extracted from:
[2] Cano et al.

How can we classify the distinct *coherent structures* of the flow and *trajectories* of the object? \Rightarrow
Bifurcation theory & Normal form reduction of the NS equations

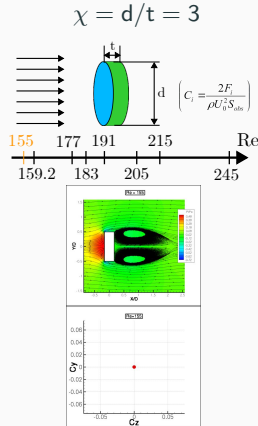
Mode interaction – Steady–Hopf – Similarities with TCF (I)

Taylor–Couette



Wake Flow past a thick disk

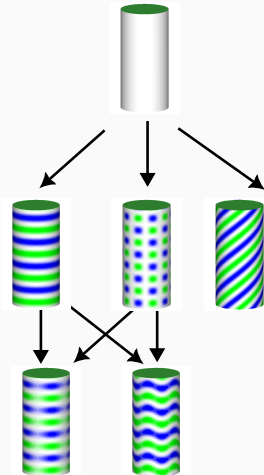
Overview of Auguste, Fabre & Magnaudet, TCFD 2009



Axisymmetric state

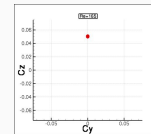
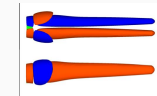
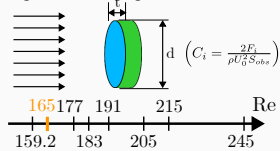
Mode interaction – Steady–Hopf – Similarities with TCF (I)

Taylor–Couette



Wake Flow past a thick disk

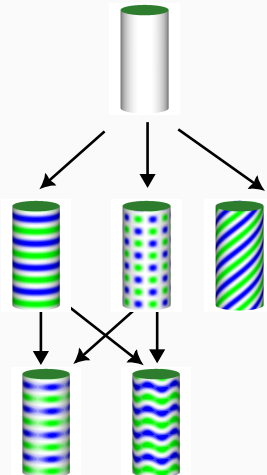
Overview of Auguste, Fabre & Magnaudet, TCFD 2009



**Steady-state state Symmetry-breaking
of the axisymmetric state**

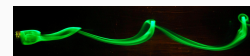
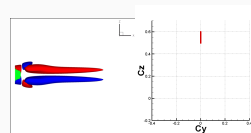
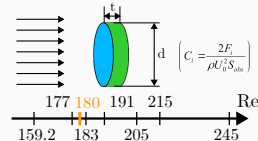
Mode interaction – Steady–Hopf – Similarities with TCF (I)

Taylor–Couette



Wake Flow past a thick disk

Overview of Auguste, Fabre & Magnaudet, TCFD 2009

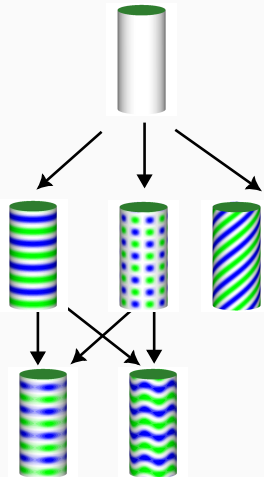


From K. Gumowski, PMMH

Zig-zig state
Periodic vortex shedding with **reflection symmetry**

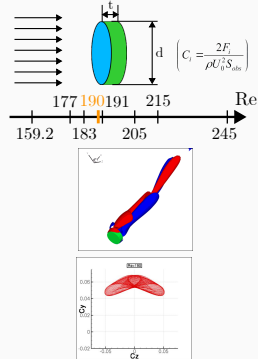
Mode interaction – Steady–Hopf – Similarities with TCF (I)

Taylor–Couette



Wake Flow past a thick disk

Overview of Auguste, Fabre & Magnaudet, TCFD 2009



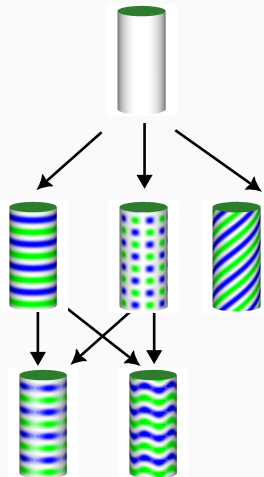
Knit-Knot state

Loss of **reflection symmetry**

Two periods: fast vortex shedding +
slow oscillation

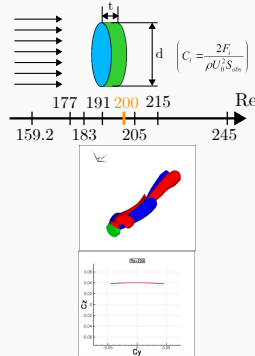
Mode interaction – Steady–Hopf – Similarities with TCF (I)

Taylor–Couette



Wake Flow past a thick disk

Overview of Auguste, Fabre & Magnaudet, TCFD 2009



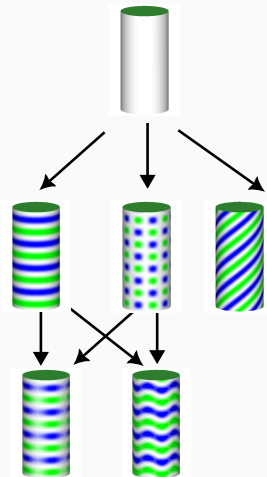
Yin-Yang state

No symmetry plane

Periodic again!

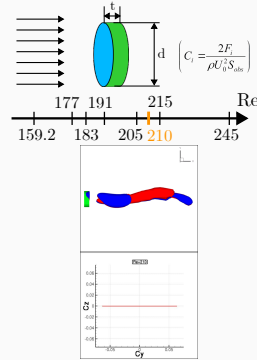
Mode interaction – Steady–Hopf – Similarities with TCF (I)

Taylor–Couette



Wake Flow past a thick disk

Overview of Auguste, Fabre & Magnaudet, TCFD 2009

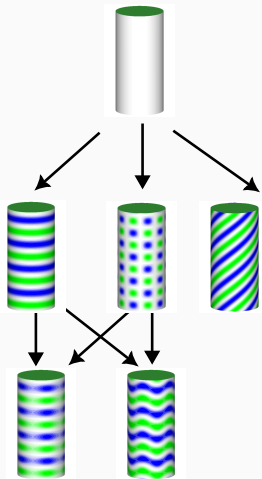


Zig-Zag state

Presence of a **symmetry plane** and periodic.

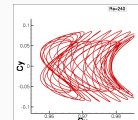
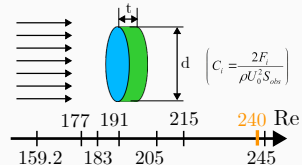
Mode interaction – Steady–Hopf – Similarities with TCF (I)

Taylor–Couette

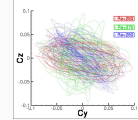


Wake Flow past a thick disk

Overview of Auguste, Fabre & Magnaudet, TCFD 2009



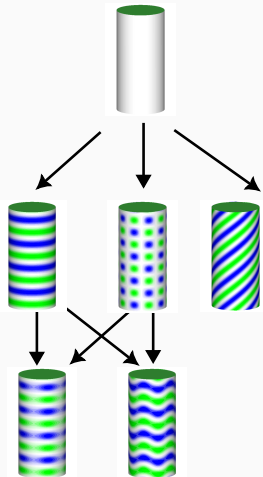
Quasiperiodic
Break-up of the
Zig-Zag



Irregular motion
Likely chaotic

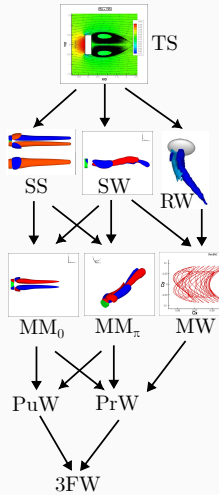
Mode interaction – Steady–Hopf – Similarities with TCF (I)

Taylor–Couette



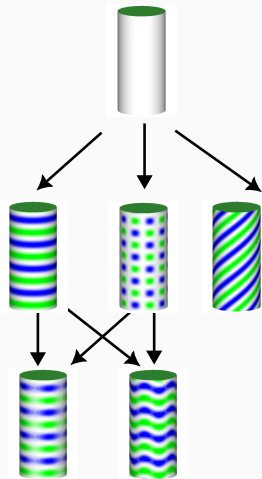
Wake Flow past a thick disk

Overview of Auguste, Fabre & Magnaudet, TCFD 2009



Mode interaction – Steady–Hopf – Similarities with TCF (I)

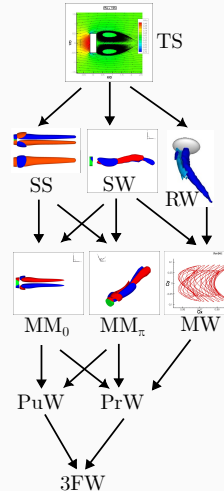
Taylor–Couette



Let's step back to classify the structures of WFA-MC problem.

Wake Flow past a thick disk

Overview of Auguète, Fabre & Magnaudet, TCFD 2009

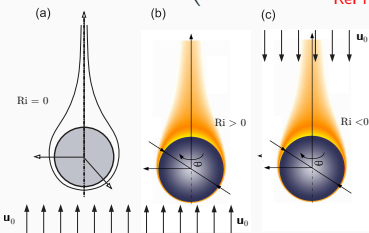


Mode interaction – Steady-Hopf – Mixed convection (Governing equations)

$$\begin{aligned}
 B \frac{\partial \mathbf{q}}{\partial t} &= \mathbf{F}(\mathbf{q}, \eta) \equiv \mathbf{L}\mathbf{q} + \mathbf{N}(\mathbf{q}, \mathbf{q}) + \mathbf{G}(\mathbf{q}, \eta), && \text{in } \Omega, \\
 \mathbf{D}_{bc} \mathbf{q}(\mathbf{x}) &= \mathbf{q}_{\partial\Omega}, && \text{on } \partial\Omega
 \end{aligned}$$

with $\mathbf{L}\mathbf{q} = \begin{pmatrix} -\nabla P \\ \nabla \cdot \mathbf{U} \\ 0 \end{pmatrix}$, $\mathbf{N}(\mathbf{q}_1, \mathbf{q}_2) = -\begin{pmatrix} \mathbf{U}_1 \cdot \nabla \mathbf{U}_2 \\ 0 \\ \mathbf{U}_1 \cdot \nabla T \end{pmatrix}$ in Ω , (2)

$$\mathbf{G}(\mathbf{q}, \eta) = \begin{pmatrix} \frac{1}{Re} \nabla \cdot (\nabla \mathbf{U} + (\nabla \mathbf{U})^T) + Ri T \mathbf{e}_z \\ 0 \\ \frac{1}{RePr} \nabla^2 T \end{pmatrix} \quad \text{in } \Omega,$$



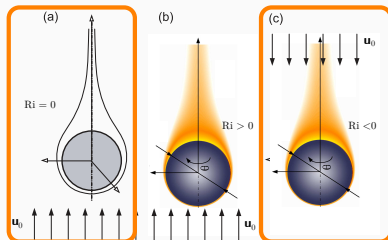
- $Re = \frac{|\mathbf{U}_\infty|d}{\nu}$
- $Ri = -\frac{\beta(\mathbf{U}_\infty \cdot \mathbf{g})(T_s - T_\infty)d}{|\mathbf{U}_\infty|^3}$
- $Pr = \frac{\nu}{\kappa}$

Mode interaction – Steady-Hopf – Mixed convection (Governing equations)

$$\begin{aligned}
 B \frac{\partial \mathbf{q}}{\partial t} &= \mathbf{F}(\mathbf{q}, \eta) \equiv \mathbf{L}\mathbf{q} + \mathbf{N}(\mathbf{q}, \mathbf{q}) + \mathbf{G}(\mathbf{q}, \eta), && \text{in } \Omega, \\
 \mathbf{D}_{bc} \mathbf{q}(x) &= \mathbf{q}_{\partial\Omega}, && \text{on } \partial\Omega
 \end{aligned}$$

with $\mathbf{L}\mathbf{q} = \begin{pmatrix} -\nabla P \\ \nabla \cdot \mathbf{U} \\ 0 \end{pmatrix}$, $\mathbf{N}(\mathbf{q}_1, \mathbf{q}_2) = -\begin{pmatrix} \mathbf{U}_1 \cdot \nabla \mathbf{U}_2 \\ 0 \\ \mathbf{U}_1 \cdot \nabla T \end{pmatrix}$ in Ω , (2)

$$\mathbf{G}(\mathbf{q}, \eta) = \begin{pmatrix} \frac{1}{Re} \nabla \cdot (\nabla \mathbf{U} + (\nabla \mathbf{U})^T) + Ri \mathbf{T} e_z \\ 0 \\ \frac{1}{RePr} \nabla^2 T \end{pmatrix} \quad \text{in } \Omega,$$



- $Re = \frac{|U_\infty|d}{\nu}$
- $Ri = -\frac{\beta(U_\infty \cdot g)(T_s - T_\infty)d}{|U_\infty|^3}$
- $Pr = \frac{\nu}{\kappa}$

Ansatz

$$\begin{aligned} \mathbf{q}(t, \tau) &= \mathbf{Q}_0 + \varepsilon \mathbf{q}_{(\varepsilon)}(t, \tau) \\ &\quad + \varepsilon^2 \mathbf{q}_{(\varepsilon^2)}(t, \tau) + O(\varepsilon^3) \\ &\equiv \mathbf{Q}_0 + \operatorname{Re}(a_0(\tau) e^{-im_0\theta} \hat{\mathbf{q}}_0) \\ &\quad + \operatorname{Re}(a_1(\tau) e^{-i\omega t} e^{-im_1\theta} \hat{\mathbf{q}}_1) \\ &\quad + \operatorname{Re}(a_2(\tau) e^{-i\omega t} e^{im_1\theta} \hat{\mathbf{q}}_2) \\ &\quad + \varepsilon^2 \mathbf{q}_{(\varepsilon^2)}(t, \tau) + O(\varepsilon^3) \end{aligned}$$

Mode interaction – Steady-Hopf – Normal form (complex form)

Ansatz

$$\begin{aligned} \mathbf{q}(t, \tau) &= \mathbf{Q}_0 + \varepsilon \mathbf{q}_{(\varepsilon)}(t, \tau) \\ &\quad + \varepsilon^2 \mathbf{q}_{(\varepsilon^2)}(t, \tau) + O(\varepsilon^3) \\ &\equiv \mathbf{Q}_0 + \operatorname{Re}(a_0(\tau) e^{-im_0\theta} \hat{\mathbf{q}}_0) \\ &\quad + \operatorname{Re}(a_1(\tau) e^{-i\omega t} e^{-im_1\theta} \hat{\mathbf{q}}_1) \\ &\quad + \operatorname{Re}(a_2(\tau) e^{-i\omega t} e^{im_1\theta} \hat{\mathbf{q}}_2) \\ &\quad + \varepsilon^2 \mathbf{q}_{(\varepsilon^2)}(t, \tau) + O(\varepsilon^3) \end{aligned}$$

Symmetries

$$\begin{aligned} \Phi &: (a_0, a_1, a_2) \rightarrow (a_0, a_1 e^{i\phi}, a_2 e^{i\phi}), \\ \kappa &: (a_0, a_1, a_2) \rightarrow (\bar{a}_0, a_2, a_1) \\ R_\alpha &: (a_0, a_1, a_2) \rightarrow (a_0 e^{i\alpha}, a_1 e^{i\alpha}, a_2 e^{-i\alpha}) \end{aligned}$$

Mode interaction – Steady-Hopf – Normal form (complex form)

Ansatz

$$\begin{aligned} \mathbf{q}(t, \tau) &= \mathbf{Q}_0 + \varepsilon \mathbf{q}_{(\varepsilon)}(t, \tau) \\ &\quad + \varepsilon^2 \mathbf{q}_{(\varepsilon^2)}(t, \tau) + O(\varepsilon^3) \\ &\equiv \mathbf{Q}_0 + \operatorname{Re}(a_0(\tau) e^{-im_0\theta} \hat{\mathbf{q}}_0) \\ &\quad + \operatorname{Re}(a_1(\tau) e^{-i\omega t} e^{-im_1\theta} \hat{\mathbf{q}}_1) \\ &\quad + \operatorname{Re}(a_2(\tau) e^{-i\omega t} e^{im_1\theta} \hat{\mathbf{q}}_2) \\ &\quad + \varepsilon^2 \mathbf{q}_{(\varepsilon^2)}(t, \tau) + O(\varepsilon^3) \end{aligned}$$

Symmetries

$$\begin{aligned} \Phi &: (a_0, a_1, a_2) \rightarrow (a_0, a_1 e^{i\phi}, a_2 e^{i\phi}), \\ \kappa &: (a_0, a_1, a_2) \rightarrow (\bar{a}_0, a_2, a_1) \\ R_\alpha &: (a_0, a_1, a_2) \rightarrow (a_0 e^{i\alpha}, a_1 e^{i\alpha}, a_2 e^{-i\alpha}) \end{aligned}$$

Normal form – Complex amplitudes

$$\begin{aligned} \dot{a}_0 &= \lambda_s a_0 + l_0 a_0 |a_0|^2 + l_1 (|a_1|^2 + |a_2|^2) a_0 \\ &\quad + i l_2 (|a_2|^2 - |a_1|^2) a_0 + l_3 \bar{a}_0 \bar{a}_2 a_1 \end{aligned}$$

$$\begin{aligned} \dot{a}_1 &= (\lambda_h + i\omega_h) a_1 + (B |a_1|^2 + (A + B) |a_2|^2) a_1 \\ &\quad + C a_1 |a_0|^2 + D a_0^2 a_2 \end{aligned}$$

$$\begin{aligned} \dot{a}_2 &= (\lambda_h + i\omega_h) a_2 + (B |a_2|^2 + (A + B) |a_1|^2) a_2 \\ &\quad + C a_2 |a_0|^2 + D \bar{a}_0^2 a_1 \end{aligned}$$

Mode interaction – Steady-Hopf – Normal form (complex form)

Ansatz

$$\begin{aligned} \mathbf{q}(t, \tau) &= \mathbf{Q}_0 + \varepsilon \mathbf{q}_{(\varepsilon)}(t, \tau) \\ &\quad + \varepsilon^2 \mathbf{q}_{(\varepsilon^2)}(t, \tau) + O(\varepsilon^3) \\ &\equiv \mathbf{Q}_0 + \operatorname{Re}(a_0(\tau) e^{-im_0\theta} \hat{\mathbf{q}}_0) \\ &\quad + \operatorname{Re}(a_1(\tau) e^{-i\omega t} e^{-im_1\theta} \hat{\mathbf{q}}_1) \\ &\quad + \operatorname{Re}(a_2(\tau) e^{-i\omega t} e^{im_1\theta} \hat{\mathbf{q}}_2) \\ &\quad + \varepsilon^2 \mathbf{q}_{(\varepsilon^2)}(t, \tau) + O(\varepsilon^3) \end{aligned}$$

Symmetries

$$\begin{aligned} \Phi &: (a_0, a_1, a_2) \rightarrow (a_0, a_1 e^{i\phi}, a_2 e^{i\phi}), \\ \kappa &: (a_0, a_1, a_2) \rightarrow (\bar{a}_0, a_2, a_1) \\ R_\alpha &: (a_0, a_1, a_2) \rightarrow (a_0 e^{i\alpha}, a_1 e^{i\alpha}, a_2 e^{-i\alpha}) \end{aligned}$$

Normal form – Complex amplitudes

$$\begin{aligned} \dot{a}_0 &= \lambda_s a_0 + l_0 a_0 |a_0|^2 + l_1 (|a_1|^2 + |a_2|^2) a_0 \\ &\quad + i l_2 (|a_2|^2 - |a_1|^2) a_0 + l_3 \bar{a}_0 \bar{a}_2 a_1 \end{aligned}$$

$$\begin{aligned} \dot{a}_1 &= (\lambda_h + i\omega_h) a_1 + (B |a_1|^2 + (A + B) |a_2|^2) a_1 \\ &\quad + C a_1 |a_0|^2 + D a_0^2 a_2 \end{aligned}$$

$$\begin{aligned} \dot{a}_2 &= (\lambda_h + i\omega_h) a_2 + (B |a_2|^2 + (A + B) |a_1|^2) a_2 \\ &\quad + C a_2 |a_0|^2 + D \bar{a}_0^2 a_1 \end{aligned}$$

The zeroth order \mathbf{Q}_0 of the reduction procedure is the steady state.

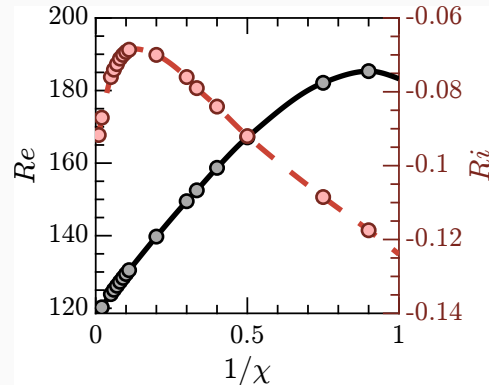
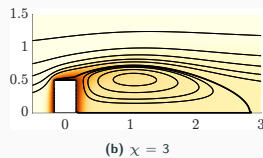
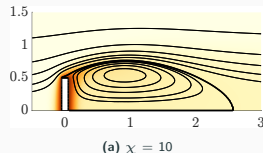
$$\begin{aligned}\mathbf{0} &= \mathbf{F}(\mathbf{Q}_0, 0), \quad x \text{ in } \Omega, \\ \mathbf{D}_{bc} \mathbf{Q}_0(x) &= \mathbf{Q}_{0,\partial\Omega}, \quad x \text{ on } \partial\Omega.\end{aligned}$$

Normal form reduction (Order 0)

The zeroth order Q_0 of the reduction procedure is the steady state.

$$\begin{aligned} Q_0 &= F(Q_0, 0), \quad x \text{ in } \Omega, \\ D_{bc} Q_0(x) &= Q_{0,\partial\Omega}, \quad x \text{ on } \partial\Omega. \end{aligned}$$

Evaluated at the threshold of instability, i.e., $\Delta\eta = 0$: **Codimension-two point**,



Normal form reduction (Order 1)

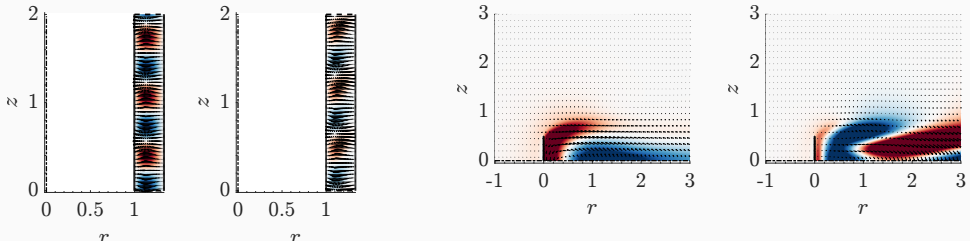
The first order solution $\mathbf{q}_{(\varepsilon)}(t, \tau)$ is composed of the eigenmodes

$$\mathbf{q}_{(\varepsilon)}(t, \tau) \equiv \operatorname{Re}(a_0(\tau)e^{-im_0\theta}\hat{\mathbf{q}}_0) + \operatorname{Re}(a_1(\tau)e^{-i\omega t}e^{-im_1\theta}\hat{\mathbf{q}}_1 + a_2(\tau)e^{-i\omega t}e^{im_2\theta}\hat{\mathbf{q}}_2) \quad (4)$$

where the reflection symmetry of $O(2)$ imposes $m_2 = -m_1$. Each term $\hat{\mathbf{q}}_\ell$ of the first order expansion is a solution of the following linear equation

$$\begin{aligned} \mathbf{J}_{(\omega_\ell, m_\ell)} \hat{\mathbf{q}}_\ell &= \left(i\omega_\ell \mathbf{B} - \frac{\partial \mathbf{F}}{\partial \mathbf{q}}|_{\mathbf{q}=\mathbf{Q}_0, \eta=0} \right) \hat{\mathbf{q}}_\ell, \quad x \text{ in } \Omega, \\ \mathbf{D}_{bc} \hat{\mathbf{q}}_\ell(x) &= 0, \quad x \text{ on } \partial\Omega. \end{aligned}$$

where $\frac{\partial \mathbf{F}}{\partial \mathbf{q}}|_{\mathbf{q}=\mathbf{Q}_0, \eta=0} \hat{\mathbf{q}}_\ell = \mathbf{L}_{m_\ell} \hat{\mathbf{q}}_\ell + \mathbf{N}_{m_\ell}(\mathbf{Q}_0, \hat{\mathbf{q}}_\ell) + \mathbf{N}_{m_\ell}(\hat{\mathbf{q}}_\ell, \mathbf{Q}_0)$.



The linear terms λ_s and λ_h are determined as follows

$$\lambda_s = \frac{\langle \hat{q}_0^\dagger, \hat{F}_{(\epsilon^3)}^{(a_0)} \rangle}{\langle \hat{q}_0^\dagger, B\hat{q}_0 \rangle}, \quad \lambda_h = \frac{\langle \hat{q}_1^\dagger, \hat{F}_{(\epsilon^3)}^{(a_1)} \rangle}{\langle \hat{q}_1^\dagger, B\hat{q}_1 \rangle} = \frac{\langle \hat{q}_2^\dagger, \hat{F}_{(\epsilon^3)}^{(a_2)} \rangle}{\langle \hat{q}_2^\dagger, B\hat{q}_2 \rangle}. \quad (5)$$

The linear terms λ_s and λ_h are determined as follows

$$\lambda_s = \frac{\langle \hat{q}_0^\dagger, \hat{F}_{(\epsilon^3)}^{(a_0)} \rangle}{\langle \hat{q}_0^\dagger, B\hat{q}_0 \rangle}, \quad \lambda_h = \frac{\langle \hat{q}_1^\dagger, \hat{F}_{(\epsilon^3)}^{(a_1)} \rangle}{\langle \hat{q}_1^\dagger, B\hat{q}_1 \rangle} = \frac{\langle \hat{q}_2^\dagger, \hat{F}_{(\epsilon^3)}^{(a_2)} \rangle}{\langle \hat{q}_2^\dagger, B\hat{q}_2 \rangle}. \quad (5)$$

The real cubic coefficients l_i for $i = 0, 1, 2, 3$ are obtained as

$$\begin{aligned} l_0 &= \frac{\langle \hat{q}_0^\dagger, \hat{F}_{(\epsilon^3)}^{(a_0|a_0|^2)} \rangle}{\langle \hat{q}_0^\dagger, B\hat{q}_0 \rangle}, & l_3 &= \frac{\langle \hat{q}_0^\dagger, \hat{F}_{(\epsilon^3)}^{(\bar{a}_0 a_1 \bar{a}_2)} \rangle}{\langle \hat{q}_0^\dagger, B\hat{q}_0 \rangle} \\ l_1 - il_2 &= \frac{\langle \hat{q}_0^\dagger, \hat{F}_{(\epsilon^3)}^{(a_0|a_1|^2)} \rangle}{\langle \hat{q}_0^\dagger, B\hat{q}_0 \rangle}, & l_1 + il_2 &= \frac{\langle \hat{q}_0^\dagger, \hat{F}_{(\epsilon^3)}^{(a_0|a_2|^2)} \rangle}{\langle \hat{q}_0^\dagger, B\hat{q}_0 \rangle}. \end{aligned} \quad (6)$$

Normal form reduction (Order 3)

The linear terms λ_s and λ_h are determined as follows

$$\lambda_s = \frac{\langle \hat{q}_0^\dagger, \hat{F}_{(\epsilon^3)}^{(a_0)} \rangle}{\langle \hat{q}_0^\dagger, B\hat{q}_0 \rangle}, \quad \lambda_h = \frac{\langle \hat{q}_1^\dagger, \hat{F}_{(\epsilon^3)}^{(a_1)} \rangle}{\langle \hat{q}_1^\dagger, B\hat{q}_1 \rangle} = \frac{\langle \hat{q}_2^\dagger, \hat{F}_{(\epsilon^3)}^{(a_2)} \rangle}{\langle \hat{q}_2^\dagger, B\hat{q}_2 \rangle}. \quad (5)$$

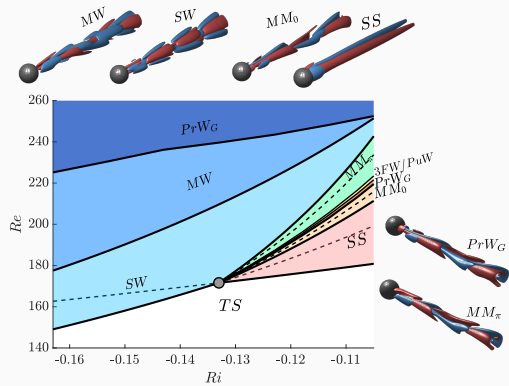
The real cubic coefficients l_i for $i = 0, 1, 2, 3$ are obtained as

$$\begin{aligned} l_0 &= \frac{\langle \hat{q}_0^\dagger, \hat{F}_{(\epsilon^3)}^{(a_0|a_0|^2)} \rangle}{\langle \hat{q}_0^\dagger, B\hat{q}_0 \rangle}, & l_3 &= \frac{\langle \hat{q}_0^\dagger, \hat{F}_{(\epsilon^3)}^{(\bar{a}_0 a_1 \bar{a}_2)} \rangle}{\langle \hat{q}_0^\dagger, B\hat{q}_0 \rangle} \\ l_1 - il_2 &= \frac{\langle \hat{q}_0^\dagger, \hat{F}_{(\epsilon^3)}^{(a_0|a_1|^2)} \rangle}{\langle \hat{q}_0^\dagger, B\hat{q}_0 \rangle}, & l_1 + il_2 &= \frac{\langle \hat{q}_0^\dagger, \hat{F}_{(\epsilon^3)}^{(a_0|a_2|^2)} \rangle}{\langle \hat{q}_0^\dagger, B\hat{q}_0 \rangle}. \end{aligned} \quad (6)$$

Finally, the complex coefficients A, B, C and D are computed as follows,

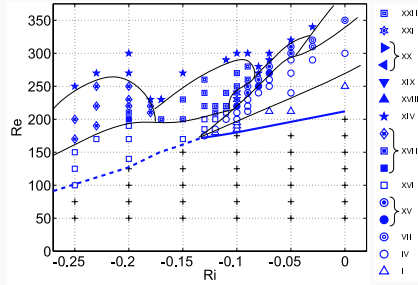
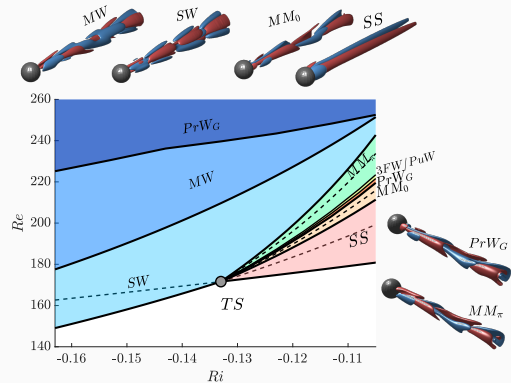
$$\begin{aligned} B &= \frac{\langle q_1^\dagger, \hat{F}_{(\epsilon^3)}^{(a_1|a_1|^2)} \rangle}{\langle \hat{q}_1^\dagger, B\hat{q}_1 \rangle}, & A + B &= \frac{\langle q_1^\dagger, \hat{F}_{(\epsilon^3)}^{(a_1|a_2|^2)} \rangle}{\langle \hat{q}_1^\dagger, B\hat{q}_1 \rangle}, \\ C &= \frac{\langle q_1^\dagger, \hat{F}_{(\epsilon^3)}^{(a_1|a_0|^2)} \rangle}{\langle \hat{q}_1^\dagger, B\hat{q}_1 \rangle}, & D &= \frac{\langle q_1^\dagger, \hat{F}_{(\epsilon^3)}^{(a_0^2 a_2)} \rangle}{\langle \hat{q}_1^\dagger, B\hat{q}_1 \rangle}. \end{aligned} \quad (7)$$

Mode interaction – Steady-Hopf – Case of the sphere (MC)



Name	Symmetry	Freq.
SS	Reflection symmetry	0
SW	Reflection symmetry	1
MM ₀	Reflection symmetry	1
MM _π	No symmetry	1
MW	No symmetry	2
PrWG	No sym. slowly rot.	2
PuW	Mean plane of sym.	2
3FW	No symmetry	3

Mode interaction – Steady-Hopf – Case of the sphere (MC)

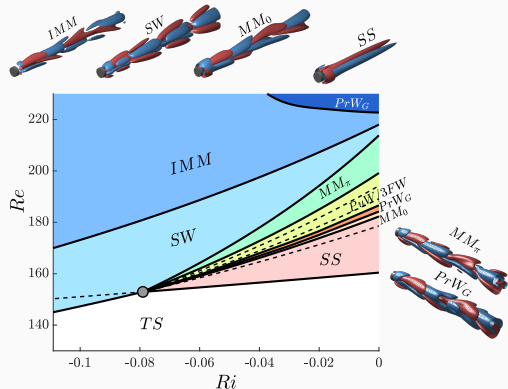


Kotouč, M. et al. (2009). Transition to turbulence in the wake of a fixed sphere in mixed convection. JFM, 625, 205–248.

Comparison

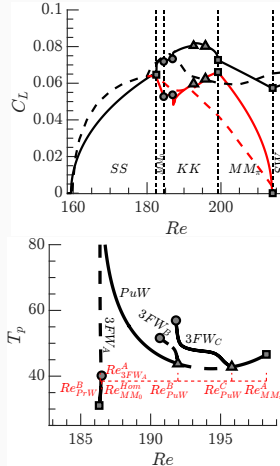
- Good quantitative matching of the primary bifurcations (SW (XVI) and SS (I)), and secondary MM₀ (IV).
- Good qualitative matching of other (secondary/tertiary) bifurcations.
- Normal form analysis allows us to establish the *intermediate states* between simulated states: MM₀(IV) and MM_π (XV). **Equivariant-bifurcation theory unveils finer details of complex spatio-temporal structures.**

Mode interaction – Steady-Hopf – Case of a thick disk



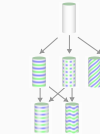
Comparison

- *Unfolding* of the Knit-Knot region.
- The second frequency of the KK region goes from $T_p \rightarrow \infty$ to (Hom. to MM_0) to $T_p \approx 40$.
- A region of *fast* transitions between PuW/PrW_G and $3FW$ s.

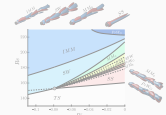


Outline

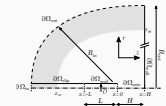
Outline of research works



Slow-fast dynamics of the wake behind bluff bodies

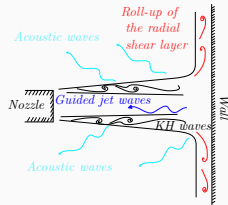
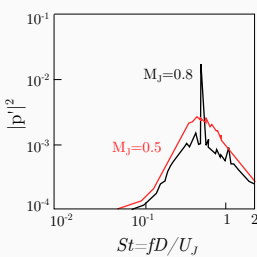


Dynamics of a rounded laminar impinging jet



Conclusion

Motivation – Apparent cut-off for broadband/tonal noise



1. Experiments by Powell^a, Ho & Noisser^b, Jaunet^c (and many others) observed:
 - Tonal sound at high subsonic Mach numbers and broadband for low Mach numbers.
2. Tam & Ahuja^d: theoretical model for the frequency selection.
 - The feedback resonance is axisymmetric if subsonic. Non-axisymmetric if supersonic.
 - Feedback between a Kelvin-Helmholtz mode and the least dispersive acoustic guided jet wave.
 - Cut-off Mach number ~ 0.6 because the $St \approx 0.7$ for the KH wave does not match the frequency of GJ mode.

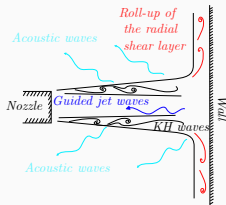
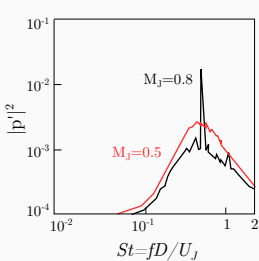
^aPowell, "On edge tones and associated phenomena".

^bHo et al., "Dynamics of an impinging jet. Part 1. The feedback phenomenon"; Nosseir et al., "Dynamics of an impinging jet. Part 2. The noise".

^cJaunet et al., "Dynamics of round jet impingement".

^dTam et al., "Theoretical model of discrete tone generation by impinging jets".

Motivation – Apparent cut-off for broadband/tonal noise



1. Experiments by Powell^a, Ho & Noisser^b, Jaunet^c (and many others) observed:
 - Tonal sound at high subsonic Mach numbers and broadband for low Mach numbers.
2. Tam & Ahuja^d: theoretical model for the frequency selection.
 - The feedback resonance is axisymmetric if subsonic. Non-axisymmetric if supersonic. ✓ Guided jet mode (0, 1) if subsonic, both (0, 1) and (1, 1) if supersonic.
 - Feedback between a Kelvin-Helmholtz mode and the least dispersive acoustic guided jet wave.
 - Cut-off Mach number ~ 0.6 because the $St \approx 0.7$ for the KH wave does not match the frequency of GJ mode.

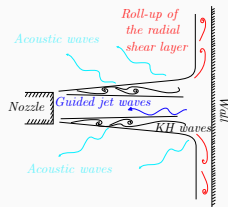
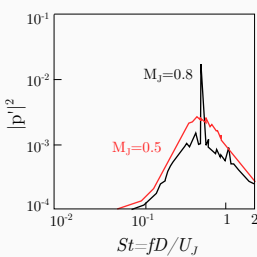
^aPowell, "On edge tones and associated phenomena".

^bHo et al., "Dynamics of an impinging jet. Part 1. The feedback phenomenon"; Nosseir et al., "Dynamics of an impinging jet. Part 2. The noise".

^cJaunet et al., "Dynamics of round jet impingement".

^dTam et al., "Theoretical model of discrete tone generation by impinging jets".

Motivation – Apparent cut-off for broadband/tonal noise



1. Experiments by Powell^a, Ho & Noisser^b, Jaunet^c (and many others) observed:
 - Tonal sound at high subsonic Mach numbers and broadband for low Mach numbers.
2. Tam & Ahuja^d: theoretical model for the frequency selection.
 - The feedback resonance is axisymmetric if subsonic. Non-axisymmetric if supersonic. ✓ **Guided jet mode (0, 1) if subsonic, both (0, 1) and (1, 1) if supersonic.**
 - Feedback between a Kelvin-Helmholtz mode and the least dispersive acoustic guided jet wave. ✓ **Derivative of the group velocity to the wavenumber is small.**
 - Cut-off Mach number ~ 0.6 because the $St \approx 0.7$ for the KH wave does not match the frequency of GJ mode.

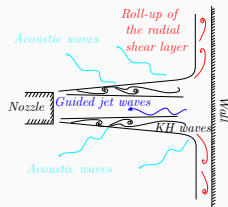
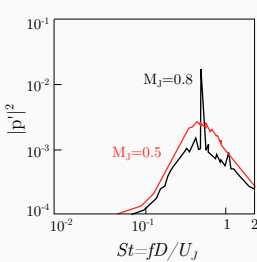
^aPowell, "On edge tones and associated phenomena".

^bHo et al., "Dynamics of an impinging jet. Part 1. The feedback phenomenon"; Nosseir et al., "Dynamics of an impinging jet. Part 2. The noise".

^cJaunet et al., "Dynamics of round jet impingement".

^dTam et al., "Theoretical model of discrete tone generation by impinging jets".

Motivation – Apparent cut-off for broadband/tonal noise



1. Experiments by Powell^a, Ho & Noisser^b, Jaunet^c (and many others) observed:
 - Tonal sound at high subsonic Mach numbers and broadband for low Mach numbers.
2. Tam & Ahuja^d: theoretical model for the frequency selection.
 - The feedback resonance is axisymmetric if subsonic. Non-axisymmetric if supersonic. ✓ Guided jet mode (0, 1) if subsonic, both (0, 1) and (1, 1) if supersonic.
 - Feedback between a Kelvin-Helmholtz mode and the least dispersive acoustic guided jet wave. ✓ Derivative of the group velocity to the wavenumber is small.
 - Cut-off Mach number ~ 0.6 because the $St \approx 0.7$ for the KH wave does not match the frequency of GJ mode. X There is a global mode for every Mach number. Yet, the physical mechanism is different at high and low Mach numbers.

^aPowell, "On edge tones and associated phenomena".

^bHo et al., "Dynamics of an impinging jet. Part 1. The feedback phenomenon"; Nosseir et al., "Dynamics of an impinging jet. Part 2. The noise".

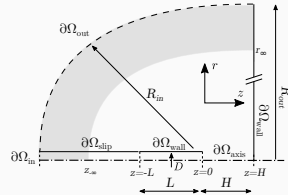
^cJaunet et al., "Dynamics of round jet impingement".

^dTam et al., "Theoretical model of discrete tone generation by impinging jets".

Dynamical system formulation

$$\mathbf{B} \frac{\partial \mathbf{q}}{\partial t} = \mathbf{F}(\mathbf{q}, \boldsymbol{\eta})$$

with $\mathbf{B} = \text{diag}(1, \rho \mathbf{I}, \rho, 0)$,



Compressible Navier–Stokes RHS (primitive variables)

$$\mathbf{F}(\mathbf{q}, \boldsymbol{\eta}) = - \begin{pmatrix} \mathbf{u} \cdot \nabla \rho + \rho \nabla \cdot \mathbf{u} \\ \rho \mathbf{u} \cdot \nabla \mathbf{u} - \nabla p + \nabla \cdot \tau(\mathbf{u}) \\ (\gamma - 1) [\rho T \nabla \cdot \mathbf{u} - \gamma M_\infty^2 \tau(\mathbf{u}) : \mathbf{D}(\mathbf{u})] + \rho \mathbf{u} \cdot \nabla T + \frac{\gamma}{\text{Pr Re}} \nabla^2 T \\ -\rho T + 1 + \gamma M_\infty^2 p \end{pmatrix},$$

Linearised Compressible Navier–Stokes RHS (primitive variables)

Non-reflecting boundary conditions \implies *Complex Mapping Technique*^a

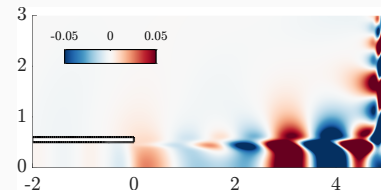
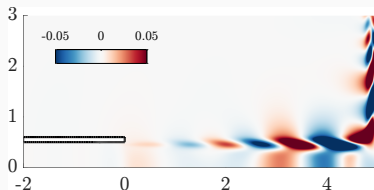
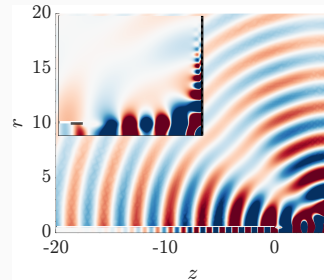
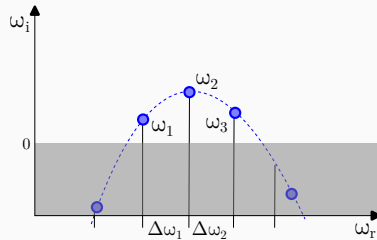
$$-i\omega \mathbf{B}|_{\mathbf{q}_0} \hat{\mathbf{q}} + \mathbf{D}\mathbf{F}|_{\mathbf{q}_0}(\hat{\mathbf{q}}) = 0$$

^aSierra-Ausin, Javier et al., "Efficient stability analysis of fluid flows using complex mapping techniques".

Linear stability (I)

Linear eigenvalue problem for the global modes

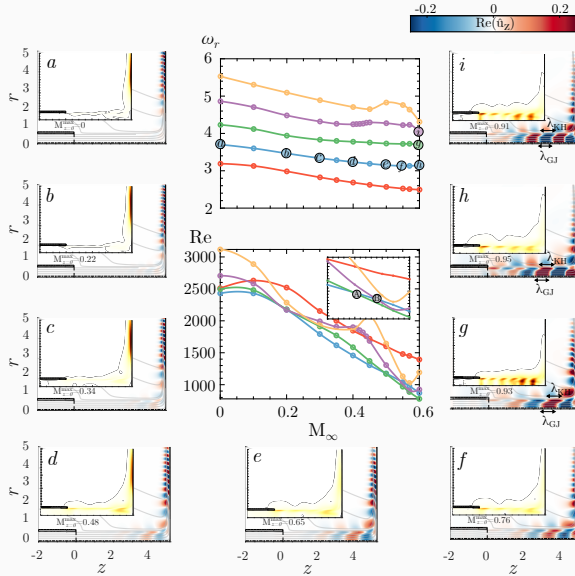
$$-i\omega B|_{q_0} \hat{q} + DF|_{q_0}(\hat{q}) = 0, \quad (8)$$



Mode interaction in external flows

Final presentation – 26/04/2023

Linear stability (II)



Decomposition of the global modes (I)

The linear perturbation \hat{q} is herein decomposed into three components: *acoustic*, *hydrodynamic* and *entropic*¹²,

Helmholtz-Hodge decomposition³

Velocity field into *acoustic* (potential) and *hydrodynamic* (solenoidal)

$$\hat{\mathbf{u}} = \hat{\mathbf{u}}_{ac} + \hat{\mathbf{u}}_{hyd} = \nabla\phi_c + \nabla \times \Psi$$

¹Ewert et al., "Acoustic perturbation equations based on flow decomposition via source filtering".

²Spieser, "Modélisation de la propagation du bruit de jet par une méthode adjointe formulée pour l'acoustique potentielle".

³Schoder et al., "Helmholtz's decomposition for compressible flows and its application to computational aeroacoustics".

Decomposition of the global modes (I)

The linear perturbation \hat{q} is herein decomposed into three components: *acoustic*, *hydrodynamic* and *entropic*¹²,

Helmholtz-Hodge decomposition³

Velocity field into *acoustic* (potential) and *hydrodynamic* (solenoidal)

$$\hat{\mathbf{u}} = \hat{\mathbf{u}}_{ac} + \hat{\mathbf{u}}_{hyd} = \nabla\phi_c + \nabla \times \Psi$$

How?

¹Ewert et al., "Acoustic perturbation equations based on flow decomposition via source filtering".

²Spieser, "Modélisation de la propagation du bruit de jet par une méthode adjointe formulée pour l'acoustique potentielle".

³Schoder et al., "Helmholtz's decomposition for compressible flows and its application to computational aeroacoustics".

Decomposition of the global modes (I)

The linear perturbation $\hat{\mathbf{q}}$ is herein decomposed into three components: *acoustic*, *hydrodynamic* and *entropic*¹²,

Helmholtz-Hodge decomposition³

Velocity field into *acoustic* (potential) and *hydrodynamic* (solenoidal)

$$\hat{\mathbf{u}} = \hat{\mathbf{u}}_{ac} + \hat{\mathbf{u}}_{hyd} = \nabla\phi_c + \nabla \times \Psi$$

How? Recover the potential ϕ_c from the Poisson equation

$$\begin{aligned}\Delta\phi_c &= \nabla \cdot \hat{\mathbf{u}} && \text{in } \Omega \\ \nabla\phi_c \cdot \mathbf{n} &= \hat{\mathbf{u}} \cdot \mathbf{n} && \text{on } \partial\Omega.\end{aligned}$$

¹Ewert et al., "Acoustic perturbation equations based on flow decomposition via source filtering".

²Spieser, "Modélisation de la propagation du bruit de jet par une méthode adjointe formulée pour l'acoustique potentielle".

³Schoder et al., "Helmholtz's decomposition for compressible flows and its application to computational aeroacoustics".

Decomposition of the global modes (I)

The linear perturbation \hat{q} is herein decomposed into three components: *acoustic*, *hydrodynamic* and *entropic*¹²,

Helmholtz-Hodge decomposition³

Velocity field into *acoustic* (potential) and *hydrodynamic* (solenoidal)

$$\hat{\mathbf{u}} = \hat{\mathbf{u}}_{ac} + \hat{\mathbf{u}}_{hyd} = \nabla\phi_c + \nabla \times \Psi$$

How? Recover the potential ϕ_c from the Poisson equation

$$\begin{aligned}\Delta\phi_c &= \nabla \cdot \hat{\mathbf{u}} && \text{in } \Omega \\ \nabla\phi_c \cdot \mathbf{n} &= \hat{\mathbf{u}} \cdot \mathbf{n} && \text{on } \partial\Omega.\end{aligned}$$

The hydrodynamic component of the velocity

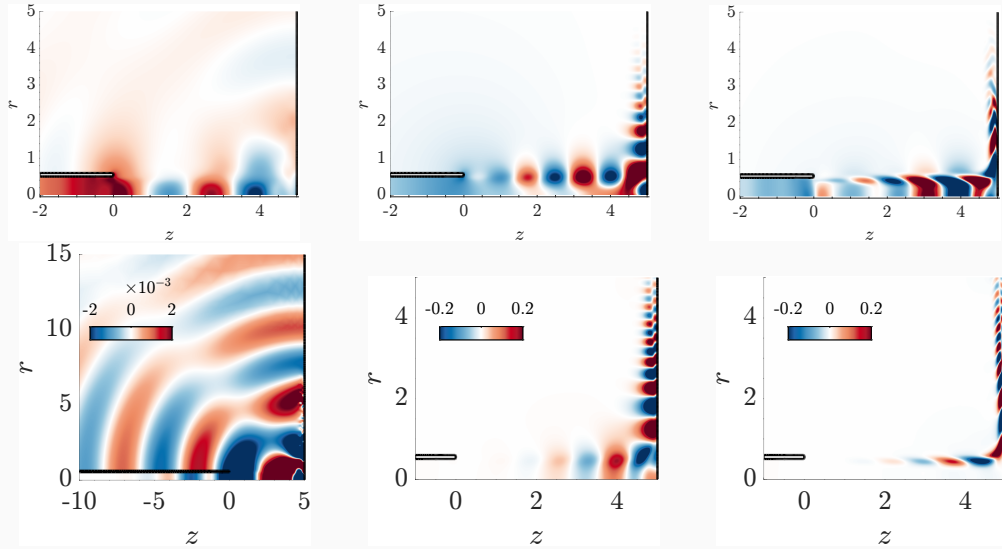
$$\hat{\mathbf{u}}_{hyd} = \hat{\mathbf{u}} - \hat{\mathbf{u}}_{ac} = \hat{\mathbf{u}} - \nabla\phi_c$$

¹Ewert et al., "Acoustic perturbation equations based on flow decomposition via source filtering".

²Spieser, "Modélisation de la propagation du bruit de jet par une méthode adjointe formulée pour l'acoustique potentielle".

³Schoder et al., "Helmholtz's decomposition for compressible flows and its application to computational aeroacoustics".

Decomposition of the global modes (II)



Wave decomposition of the main feedback (I)

We perform the weakly non-parallel expansion

$$\mathbf{q}(r, z) = [\mathbf{u}, p, T, \rho]^T(r, z) = \epsilon^n e^{\frac{i}{\epsilon} \int \alpha(z) dz} \sum \tilde{\mathbf{q}}_n(r)$$

Wave decomposition of the main feedback (I)

We perform the weakly non-parallel expansion

$$\mathbf{q}(r, z) = [\mathbf{u}, p, T, \rho]^T(r, z) = \epsilon^n e^{\frac{i}{\epsilon} \int \alpha(z) dz} \sum \tilde{\mathbf{q}}_n(r)$$

Determined from a multiple scales analysis

$$\begin{array}{lll} O(0) & (-i\omega \mathbf{B} + D\mathbf{F}(\alpha))\tilde{\mathbf{q}}_0 & \text{Eig. problem for } \alpha \\ O(\epsilon) & (-i\omega \mathbf{B} + D\mathbf{F}(\alpha))\tilde{\mathbf{q}}_1 = i \frac{d}{d\alpha} (-i\omega \mathbf{B} + D\mathbf{F}(\alpha)) \frac{\tilde{\mathbf{q}}_0}{dz} & \text{Forced problem} \end{array} \quad (9)$$

Wave decomposition of the main feedback (I)

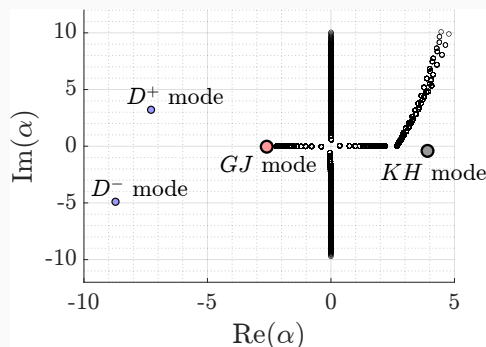
We perform the weakly non-parallel expansion

$$\mathbf{q}(r, z) = [\mathbf{u}, p, T, \rho]^T(r, z) = \epsilon^n e^{\frac{i}{\epsilon} \int \alpha(z) dz} \sum \tilde{\mathbf{q}}_n(r)$$

Determined from a multiple scales analysis

$O(0)$	$(-i\omega \mathbf{B} + D\mathbf{F}(\alpha))\tilde{\mathbf{q}}_0$	Eig. problem for α
$O(\epsilon)$	$(-i\omega \mathbf{B} + D\mathbf{F}(\alpha))\tilde{\mathbf{q}}_1 = i \frac{d}{d\alpha} (-i\omega \mathbf{B} + D\mathbf{F}(\alpha)) \frac{\tilde{\mathbf{q}}_0}{dz}$	Forced problem

(9)



Wave decomposition of the main feedback (I)

We perform the weakly non-parallel expansion

$$\mathbf{q}(r, z) = [\mathbf{u}, p, T, \rho]^T(r, z) = \epsilon^n e^{\frac{i}{\epsilon} \int \alpha(z) dz} \sum \tilde{\mathbf{q}}_n(r)$$

Determined from a multiple scales analysis

$$\begin{array}{ll} O(0) & (-i\omega \mathbf{B} + D\mathbf{F}(\alpha)) \tilde{\mathbf{q}}_0 \\ O(\epsilon) & (-i\omega \mathbf{B} + D\mathbf{F}(\alpha)) \tilde{\mathbf{q}}_1 = i \frac{d}{d\alpha} (-i\omega \mathbf{B} + D\mathbf{F}(\alpha)) \frac{\tilde{\mathbf{q}}_0}{dz} \end{array} \quad \begin{array}{l} \text{Eig. problem for } \alpha \\ \text{Forced problem} \end{array} \quad (9)$$

After imposing solvability condition

$$\mathbf{q}(z) = C_0 e^{i \int \alpha + \delta \alpha dz} \tilde{\mathbf{q}}_0 \text{ where } \delta \alpha = \frac{\tilde{\mathbf{q}}_0^\dagger \cdot \left[\frac{d}{d\alpha} (-i\omega \mathbf{B} + D\mathbf{F}(\alpha)) \frac{\tilde{\mathbf{q}}_0}{dz} \right]}{\tilde{\mathbf{q}}_0^\dagger \cdot \left[\frac{d}{d\alpha} (-i\omega \mathbf{B} + D\mathbf{F}(\alpha)) \tilde{\mathbf{q}}_0 \right]}$$

Then we can expand the linear global mode in a weakly non-parallel basis

$$\hat{\mathbf{q}} \approx \sum_k C_{0,k} e^{i \int \alpha_k + \delta \alpha_k dz} \tilde{\mathbf{q}}_{0,k}$$

then finally,

$$C_{0,k} \approx \tilde{\mathbf{q}}_0^\dagger \cdot \left[\frac{d}{d\alpha} (-i\omega \mathbf{B} + D\mathbf{F}(\alpha)) \hat{\mathbf{q}} \right] e^{-i \int \alpha_k + \delta \alpha_k dz}$$

Wave decomposition of the main feedback (II)

Expand the linear global mode in a weakly non-parallel basis

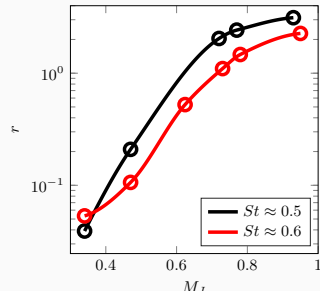
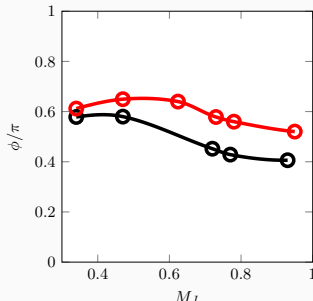
$$\hat{\mathbf{q}} \approx \sum_k C_{0,k} e^{i \int \alpha_k + \delta \alpha_k dz} \tilde{\mathbf{q}}_{0,k}$$

with,

$$C_{0,k} \approx \tilde{\mathbf{q}}_0^\dagger \cdot \left[\frac{d}{d\alpha} (-i\omega \mathbf{B} + D\mathbf{F}(\alpha)) \hat{\mathbf{q}} \right] e^{-i \int \alpha_k + \delta \alpha_k dz}$$

We can determine the reflection coefficient as

$$r e^{i\phi} = C_{0,GJ} / C_{0,KH}$$



How does change the instability change by a small spatially localised linear harmonic feedback term
 $H(\hat{q}) \equiv \delta(x - x_0) P_H C_0 P_{\hat{q}} \hat{q}$?

Structural sensitivity

Introduce a harmonic forcing term

$$\left(-i\omega B|_{q_0} + DF|_{q_0} \right) \hat{q} = H(\hat{q}). \quad (10)$$

S_s measures the variation of the eigenvalue w.r.t. to the forcing.

$$i\delta\omega = \langle P_H \hat{q}^\dagger, \delta(x - x_0) C_0 P_{\hat{q}} \hat{q} \rangle \leq \|C_0\| \|P_H \hat{q}^\dagger\|_{L^2} \|P_{\hat{q}} \hat{q}\|_{L^2} = \|C_0\| S_s(x_0), \quad (11)$$

Non-local structural sensitivity decomposition

How does change the instability change by a small spatially localised linear harmonic feedback term
 $H(\hat{q}) \equiv \delta(x - x_0) P_H C_0 P_{\hat{q}} \hat{q}$?

Structural sensitivity

Introduce a harmonic forcing term

$$\left(-i\omega B|_{q_0} + DF|_{q_0} \right) \hat{q} = H(\hat{q}). \quad (10)$$

S_s measures the variation of the eigenvalue w.r.t. to the forcing. **Decompose it!**

$$i\delta\omega = \langle P_H \hat{q}^\dagger, \delta(x - x_0) C_0 P_{\hat{q}} \hat{q} \rangle \leq \|C_0\| \|P_H \hat{q}^\dagger\|_{L^2} \|P_{\hat{q}} \hat{q}\|_{L^2} = \|C_0\| S_s(x_0), \quad (11)$$

Decomposition of the mode

$$H(\hat{q}) = H(\hat{q}_{ac}) + H(\hat{q}_{hyd}) + H(\hat{q}_s). \quad (12)$$

Non-local structural sensitivity decomposition

How does change the instability change by a small spatially localised linear harmonic feedback term
 $H(\hat{q}) \equiv \delta(x - x_0) P_H C_0 P_{\hat{q}} \hat{q}$?

Structural sensitivity

Introduce a harmonic forcing term

$$\left(-i\omega B|_{q_0} + DF|_{q_0} \right) \hat{q} = H(\hat{q}). \quad (10)$$

S_s measures the variation of the eigenvalue w.r.t. to the forcing. **Decompose it!**

$$i\delta\omega = \langle P_H \hat{q}^\dagger, \delta(x - x_0) C_0 P_{\hat{q}} \hat{q} \rangle \leq \|C_0\| \|P_H \hat{q}^\dagger\|_{L^2} \|P_{\hat{q}} \hat{q}\|_{L^2} = \|C_0\| S_s(x_0), \quad (11)$$

Decomposition of the mode

$$H(\hat{q}) = H(\hat{q}_{ac}) + H(\hat{q}_{hyd}) + H(\hat{q}_s). \quad (12)$$

Does $H(\hat{q}_{ac})$ induce *hydrodynamic* perturbations ?

Non-local structural sensitivity decomposition

How does change the instability change by a small spatially localised linear harmonic feedback term
 $H(\hat{q}) \equiv \delta(x - x_0) P_H C_0 P_{\hat{q}} \hat{q}$?

Structural sensitivity

Introduce a harmonic forcing term

$$\left(-i\omega B|_{q_0} + DF|_{q_0} \right) \hat{q} = H(\hat{q}). \quad (10)$$

S_s measures the variation of the eigenvalue w.r.t. to the forcing. **Decompose it!**

$$i\delta\omega = \langle P_H \hat{q}^\dagger, \delta(x - x_0) C_0 P_{\hat{q}} \hat{q} \rangle \leq \|C_0\| \|P_H \hat{q}^\dagger\|_{L^2} \|P_{\hat{q}} \hat{q}\|_{L^2} = \|C_0\| S_s(x_0), \quad (11)$$

Decomposition of the mode

$$H(\hat{q}) = H(\hat{q}_{ac}) + H(\hat{q}_{hyd}) + H(\hat{q}_s). \quad (12)$$

Does $H(\hat{q}_{ac})$ induce *hydrodynamic* perturbations ?

$$\begin{aligned} & \frac{\partial \hat{\omega}}{\partial t} + \mathbf{u}_0 \cdot \nabla \hat{\omega} + \hat{\mathbf{u}} \cdot \nabla \omega_0 + \omega_0 (\nabla \cdot \hat{\mathbf{u}}) + \hat{\omega} (\nabla \cdot \mathbf{u}_0) - \\ & \frac{1}{\rho_0^2} \nabla p_0 \times \nabla \hat{p} + \frac{1}{\rho_0^2} \nabla \hat{p} \times \nabla p_0 - \nabla \times (\tau(\hat{\mathbf{u}})/\rho_0) = \nabla \times \mathbf{H}_u(\mathbf{u}) \end{aligned}$$

Non-local structural sensitivity decomposition

How does change the instability change by a small spatially localised linear harmonic feedback term
 $\mathbf{H}(\hat{\mathbf{q}}) \equiv \delta(x - x_0) \mathbf{P}_H \mathbf{C}_0 \mathbf{P}_{\hat{\mathbf{q}}} \hat{\mathbf{q}}$?

Structural sensitivity

Introduce a harmonic forcing term

$$\left(-i\omega \mathbf{B}|_{\mathbf{q}_0} + \mathbf{D}\mathbf{F}|_{\mathbf{q}_0} \right) \hat{\mathbf{q}} = \mathbf{H}(\hat{\mathbf{q}}). \quad (10)$$

\mathbf{S}_s measures the variation of the eigenvalue w.r.t. to the forcing. **Decompose it!**

$$i\delta\omega = \langle \mathbf{P}_H \hat{\mathbf{q}}^\dagger, \delta(x - x_0) \mathbf{C}_0 \mathbf{P}_{\hat{\mathbf{q}}} \hat{\mathbf{q}} \rangle \leq \|\mathbf{C}_0\| \|\mathbf{P}_H \hat{\mathbf{q}}^\dagger\|_{L^2} \|\mathbf{P}_{\hat{\mathbf{q}}} \hat{\mathbf{q}}\|_{L^2} = \|\mathbf{C}_0\| \mathbf{S}_s(x_0), \quad (11)$$

Decomposition of the mode

$$\mathbf{H}(\hat{\mathbf{q}}) = \mathbf{H}(\hat{\mathbf{q}}_{ac}) + \mathbf{H}(\hat{\mathbf{q}}_{hyd}) + \mathbf{H}(\hat{\mathbf{q}}_s). \quad (12)$$

Does $\mathbf{H}(\hat{\mathbf{q}}_{ac})$ induce *hydrodynamic* perturbations ?

$$\begin{aligned} & \frac{\partial \hat{\omega}}{\partial t} + \mathbf{u}_0 \cdot \nabla \hat{\omega} + \hat{\mathbf{u}} \cdot \nabla \omega_0 + \omega_0 (\nabla \cdot \hat{\mathbf{u}}) + \hat{\omega} (\nabla \cdot \mathbf{u}_0) - \\ & \frac{1}{\rho_0^2} \nabla p_0 \times \nabla \hat{\rho} + \frac{1}{\rho_0^2} \nabla \hat{\rho} \times \nabla p_0 - \nabla \times (\tau(\hat{\mathbf{u}})/\rho_0) = \nabla \times \mathbf{H}_u(\mathbf{u}) \end{aligned}$$

The forcing term must be rotational-free, i.e., $\nabla \times \mathbf{H}(\mathbf{u}_{ac}) = 0$

Non-local structural sensitivity decomposition

How does change the instability change by a small spatially localised linear harmonic feedback term
 $H(\hat{q}) \equiv \delta(x - x_0) P_H C_0 P_{\hat{q}} \hat{q}$?

Structural sensitivity

Introduce a harmonic forcing term

$$\left(-i\omega B|_{q_0} + DF|_{q_0} \right) \hat{q} = H(\hat{q}). \quad (10)$$

S_s measures the variation of the eigenvalue w.r.t. to the forcing. **Decompose it!**

$$i\delta\omega = \langle P_H \hat{q}^\dagger, \delta(x - x_0) C_0 P_{\hat{q}} \hat{q} \rangle \leq \|C_0\| \|P_H \hat{q}^\dagger\|_{L^2} \|P_{\hat{q}} \hat{q}\|_{L^2} = \|C_0\| S_s(x_0), \quad (11)$$

Decomposition of the adjoint mode

$$H = H_{ac} + H_{hyd} + H_s$$

Non-local structural sensitivity decomposition

How does change the instability change by a small spatially localised linear harmonic feedback term
 $H(\hat{q}) \equiv \delta(x - x_0) P_H C_0 P_{\hat{q}} \hat{q}$?

Structural sensitivity

Introduce a harmonic forcing term

$$\left(-i\omega B|_{q_0} + DF|_{q_0} \right) \hat{q} = H(\hat{q}). \quad (10)$$

S_s measures the variation of the eigenvalue w.r.t. to the forcing. **Decompose it!**

$$i\delta\omega = \langle P_H \hat{q}^\dagger, \delta(x - x_0) C_0 P_{\hat{q}} \hat{q} \rangle \leq \|C_0\| \|P_H \hat{q}^\dagger\|_{L^2} \|P_{\hat{q}} \hat{q}\|_{L^2} = \|C_0\| S_s(x_0), \quad (11)$$

Decomposition of the adjoint mode

$$H = H_{ac} + H_{hyd} + H_s$$

If no mass injection, direct-adjoint decomposition is **bi-orthogonal**, so $H_{ac}(\hat{q}) = \langle \hat{q}_{ac}^\dagger, H(\hat{q}) \rangle \hat{q}_{ac}$,
 $H_{hyd}(\hat{q}) = \langle \hat{q}_{hyd}^\dagger, H(\hat{q}) \rangle \hat{q}_{hyd}$ and $H_s(\hat{q}) = \langle \hat{q}_s^\dagger, H(\hat{q}) \rangle \hat{q}_s$

Non-local structural sensitivity decomposition

How does change the instability change by a small spatially localised linear harmonic feedback term
 $H(\hat{q}) \equiv \delta(x - x_0) P_H C_0 P_{\hat{q}} \hat{q}$?

Structural sensitivity

Introduce a harmonic forcing term

$$\left(-i\omega B|_{q_0} + DF|_{q_0} \right) \hat{q} = H(\hat{q}). \quad (10)$$

S_s measures the variation of the eigenvalue w.r.t. to the forcing. **Decompose it!**

$$i\delta\omega = \langle P_H \hat{q}^\dagger, \delta(x - x_0) C_0 P_{\hat{q}} \hat{q} \rangle \leq \|C_0\| \|P_H \hat{q}^\dagger\|_{L^2} \|P_{\hat{q}} \hat{q}\|_{L^2} = \|C_0\| S_s(x_0), \quad (11)$$

Decomposition of the adjoint mode

$$H = H_{ac} + H_{hyd} + H_s$$

If no mass injection, direct-adjoint decomposition is **bi-orthogonal**, so $H_{ac}(\hat{q}) = \langle \hat{q}_{ac}, H(\hat{q}) \rangle \hat{q}_{ac}$,
 $H_{hyd}(\hat{q}) = \langle \hat{q}_{hyd}^\dagger, H(\hat{q}) \rangle \hat{q}_{hyd}$ and $H_s(\hat{q}) = \langle \hat{q}_s^\dagger, H(\hat{q}) \rangle \hat{q}_s$

$$\begin{cases} -i\omega B|_{q_0} + DF|_{q_0} + \langle \hat{q}_{ac}^\dagger, H(\hat{q}_{ac}) \rangle + \langle \hat{q}_{ac}^\dagger, H(\hat{q}_{hyd}) \rangle + \langle \hat{q}_{ac}^\dagger, H(\hat{q}_s) \rangle \hat{q}_{ac} = 0 \\ -i\omega B|_{q_0} + DF|_{q_0} + \langle \hat{q}_{hyd}^\dagger, H(\hat{q}_{ac}) \rangle + \langle \hat{q}_{hyd}^\dagger, H(\hat{q}_{hyd}) \rangle + \langle \hat{q}_{hyd}^\dagger, H(\hat{q}_s) \rangle \hat{q}_{hyd} = 0 \\ -i\omega B|_{q_0} + DF|_{q_0} + \langle \hat{q}_s^\dagger, H(\hat{q}_{ac}) \rangle + \langle \hat{q}_s^\dagger, H(\hat{q}_{hyd}) \rangle + \langle \hat{q}_s^\dagger, H(\hat{q}_s) \rangle \hat{q}_s = 0, \end{cases}$$

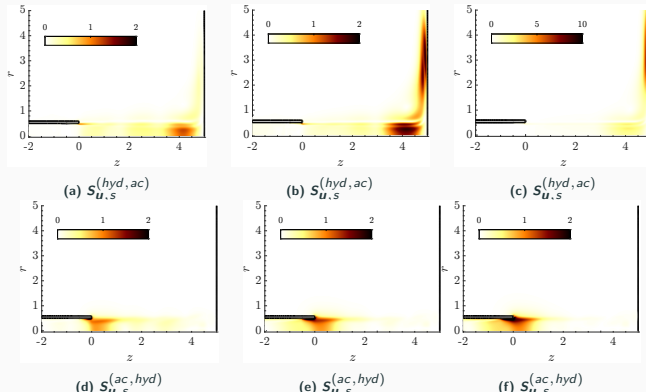
Non-local structural sensitivity decomposition

Non-local Structural sensitivity

Introduce a harmonic forcing term

$$\left(-i\omega B|_{q_0} + DF|_{q_0} \right) \hat{q} = H(\hat{q}). \quad (10)$$

$$\begin{aligned} i\delta\omega_j^k &= \langle \hat{q}_k^\dagger, \delta(x - x_0) C_0 \hat{q}_j \rangle \leq \|C_0\| \| \hat{q}_k^\dagger(x_0) \| \| \hat{q}_j(x_0) \| = \|C_0\| S^{(j,k)}_s(x_0), \\ S^{(j,k)}_s(x_0) &= \| \hat{q}_k^\dagger(x_0) \| \| \hat{q}_j(x_0) \| \text{ with } j, k = \text{ac, hyd, s}. \end{aligned}$$



Mode interaction in external flows

Final presentation – 26/04/2023

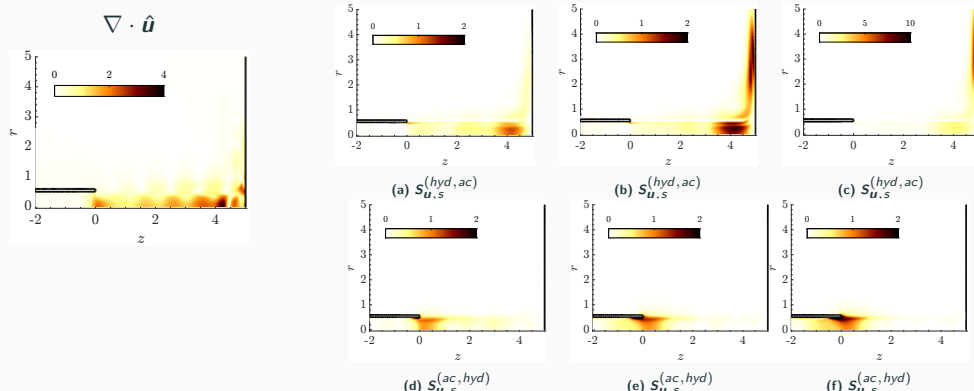
Non-local structural sensitivity decomposition

Non-local Structural sensitivity

Introduce a harmonic forcing term

$$\left(-i\omega B|_{q_0} + DF|_{q_0} \right) \hat{q} = H(\hat{q}). \quad (10)$$

$$\begin{aligned} i\delta\omega_j^k &= \langle \hat{q}_k^\dagger, \delta(x - x_0) C_0 \hat{q}_j \rangle \leq \|C_0\| \| \hat{q}_k^\dagger(x_0) \| \| \hat{q}_j(x_0) \| = \|C_0\| S^{(j,k)}_s(x_0), \\ S^{(j,k)}_s(x_0) &= \| \hat{q}_k^\dagger(x_0) \| \| \hat{q}_j(x_0) \| \text{ with } j, k = \text{ac, hyd, s}. \end{aligned}$$



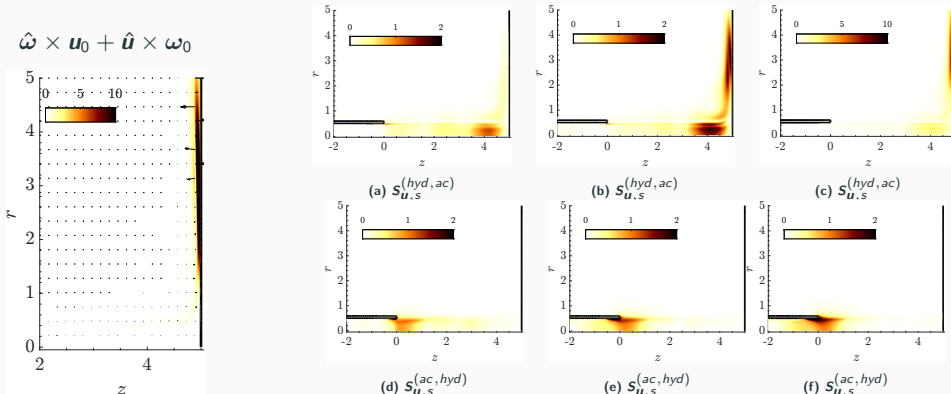
Non-local structural sensitivity decomposition

Non-local Structural sensitivity

Introduce a harmonic forcing term

$$\left(-i\omega B|_{q_0} + DF|_{q_0} \right) \hat{q} = H(\hat{q}). \quad (10)$$

$$\begin{aligned} i\delta\omega_j^k &= \langle \hat{q}_k^\dagger, \delta(x - x_0) C_0 \hat{q}_j \rangle \leq \|C_0\| \| \hat{q}_k^\dagger(x_0) \| \| \hat{q}_j(x_0) \| = \|C_0\| S^{(j,k)}_s(x_0), \\ S^{(j,k)}_s(x_0) &= \| \hat{q}_k^\dagger(x_0) \| \| \hat{q}_j(x_0) \| \text{ with } j, k = \text{ac, hyd, s}. \end{aligned}$$

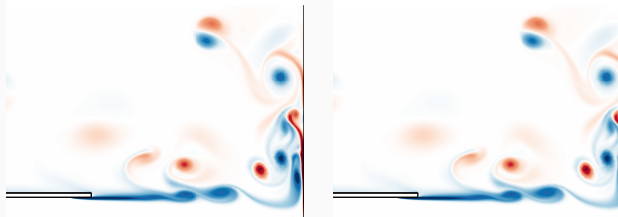


Broadband-tonal sound in subsonic rounded impinging jet (I)

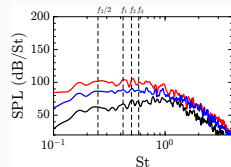
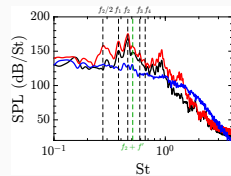
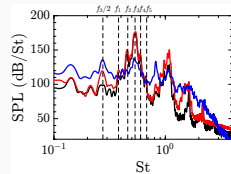
Main cases observed from the axisymmetric *DNS*

(a) Tonal resonance:

- (i) For Monochromatic dynamics: Strict monochromatic dynamics only near transition. Larger interval for large subsonic Mach numbers.
 - (ii) Quasi-periodic resonance: Two incommensurate frequencies lead to the excitation of every (unstable) global mode, which are phase-locked.
- (b) Hopf bifurcation of the case (a.ii): Slow desynchronization of the quasi-periodic attractor with a slow frequency $f' \propto \delta\omega$, it occurs for $0.4 < M_J < 0.9$
- (c) Route towards chaos/broadband near the onset of linear instability, it occurs for $M_J < 0.4$

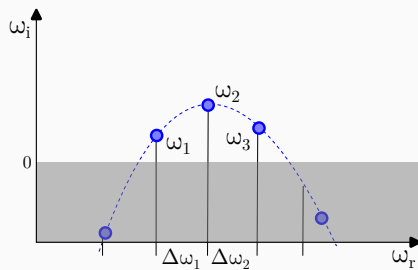


Mode interaction in external flows



Findings from linear stability

- Spectrum displays nearly *equi-distant* (in frequency) eigenvalues.



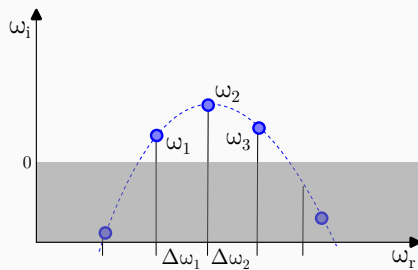
Modelling of the interaction

$$\mathbf{q} = \mathbf{q}_0 + \sum_{j=1}^N [r_j e^{i\phi_j(t)} \hat{\mathbf{q}} + \text{c.c.}] + \text{higher harmonics}$$

⁴Verified with WNL and we did not observe subcriticality via time-stepping simulations.

Findings from linear stability

- Spectrum displays nearly *equi-distant* (in frequency) eigenvalues.
- We consider the *simplest scenario* of $N = 3$ unstable modes.



Modelling of the interaction

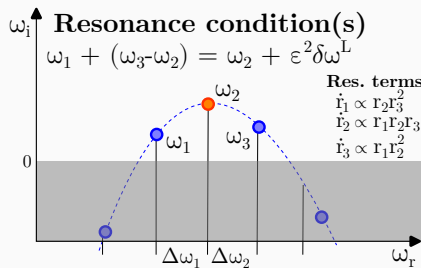
$$\mathbf{q} = \mathbf{q}_0 + \sum_{j=1}^N [r_j e^{i\phi_j(t)} \hat{\mathbf{q}} + \text{c.c.}] + \text{higher harmonics}$$

$$\begin{aligned}\dot{r}_j &= r_j [\lambda_j + \sum_k^N \text{Re}(\nu_{jk}) r_k^2] \\ \dot{\phi}_j &= \omega_j + \sum_k^N \text{Im}(\nu_{jk}) r_k^2\end{aligned}$$

⁴Verified with WNL and we did not observe subcriticality via time-stepping simulations.

Findings from linear stability

- Spectrum displays nearly *equi-distant* (in frequency) eigenvalues.
 - We consider the *simplest scenario* of $N = 3$ unstable modes.
 - The nearly equidistant condition imposes a *resonant condition*.



Modelling of the interaction

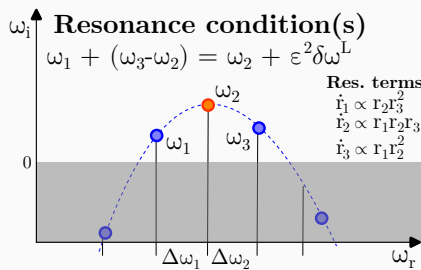
$$\mathbf{q} = \mathbf{q}_0 + \sum_{j=1}^N [r_j e^{i\phi_j(t)} \hat{\mathbf{q}} + \text{c.c.}] + \text{higher harmonics}$$

$$\begin{aligned}\dot{r}_j &= r_j [\lambda_j + \sum_k^N \text{Re}(\nu_{jk}) r_k^2] + f_r(r, \phi) \\ \dot{\phi}_j &= \omega_j + \sum_k^N \text{Im}(\nu_{jk}) r_k^2 + f_{\phi_j}(r, \phi)\end{aligned}$$

⁴Verified with WNL and we did not observe subcriticality via time-stepping simulations.

Findings from linear stability

- Spectrum displays nearly *equi-distant* (in frequency) eigenvalues.
 - We consider the *simplest scenario* of $N = 3$ unstable modes.
 - The nearly equidistant condition imposes a *resonant condition*.
- They correspond to *supercritical*⁴ Hopf bifurcations.



Modelling of the interaction

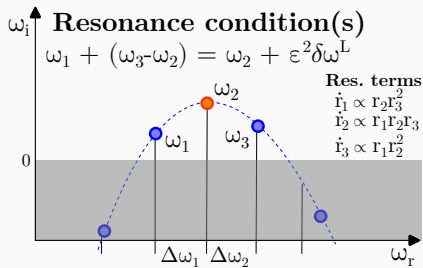
$$\mathbf{q} = \mathbf{q}_0 + \sum_{j=1}^N [r_j e^{i\phi_j(t)} \hat{\mathbf{q}} + \text{c.c.}] + \text{higher harmonics}$$

$$\begin{aligned}\dot{r}_j &= r_j \left[\lambda_j + \underbrace{\sum_k \text{Re}(\nu_{jk}) r_k^2}_{\text{Re}(\nu_{jj}) < 0} \right] + f_{r_j}(\mathbf{r}, \phi) \\ \dot{\phi}_j &= \omega_j + \sum_k \text{Im}(\nu_{jk}) r_k^2 + f_{\phi_j}(\mathbf{r}, \phi)\end{aligned}$$

⁴Verified with WNL and we did not observe subcriticality via time-stepping simulations.

Findings from linear stability

- Spectrum displays nearly *equi-distant* (in frequency) eigenvalues.
 - We consider the *simplest scenario* of $N = 3$ unstable modes.
 - The nearly equidistant condition imposes a *resonant condition*.
- They correspond to *supercritical*⁴ Hopf bifurcations.
- The resonance condition imposes a resonant phase $\Psi = \phi_1 + \phi_3 - 2\phi_2$.



Modelling of the interaction

$$\mathbf{q} = \mathbf{q}_0 + \sum_{j=1}^N [r_j e^{i\phi_j(t)} \hat{\mathbf{q}} + \text{c.c.}] + \text{higher harmonics}$$

$$\begin{aligned}\dot{r}_j &= r_j [\lambda_j + \sum_k^N \text{Re}(\nu_{jk}) r_k^2] + f_{r_j}(\mathbf{r}, \phi) \\ \dot{\Psi} &= \delta\omega + f_\Psi(\mathbf{r}, \phi)\end{aligned}$$

$$\begin{aligned}\delta\omega &\equiv \delta\omega^L + \delta\omega^{NL} \text{ with } \delta\omega^L \equiv [\omega_1 + \omega_3 - 2\omega_2] \\ \delta\omega^{NL} &\equiv \Delta\omega_2^{NL} - \Delta\omega_1^{NL} = [\omega_1^{NL} + \omega_3^{NL} - 2\omega_2^{NL}], \text{ where} \\ \omega_k^{NL} &= \lambda'_k + \nu'_{k1} r_1^2 + \nu'_{k2} r_2^2 + \nu'_{k3} r_3^2.\end{aligned}$$

⁴Verified with WNL and we did not observe subcriticality via time-stepping simulations.

Modelling of the interaction

$$\begin{aligned}\dot{r}_j &= r_j [\lambda_j + \sum_k^N \operatorname{Re}(\nu_{jk}) r_k^2] + f_r(r, \phi) \\ \dot{\psi} &= \delta\omega + f_\psi(r, \phi)\end{aligned}$$

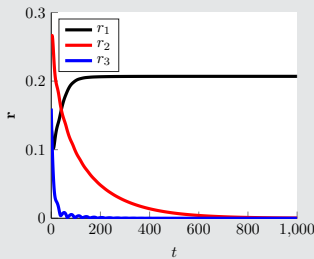
$\delta\omega \equiv \delta\omega^L + \delta\omega^{NL}$ with $\delta\omega^L \equiv [\omega_1 + \omega_3 - 2\omega_2]$ and $\delta\omega^{NL} \equiv [\omega_1^{NL} + \omega_3^{NL} - 2\omega_2^{NL}]$, where
 $\omega_k^{NL} = \lambda'_k + \nu'_{k1} r_1^2 + \nu'_{k2} r_2^2 + \nu'_{k3} r_3^2$.

Modelling of the interaction

$$\begin{aligned}\dot{r}_j &= r_j [\lambda_j + \sum_k^N \operatorname{Re}(\nu_{jk}) r_k^2] + f_{r_j}(r, \phi) \\ \dot{\psi} &= \delta\omega + f_\psi(r, \phi)\end{aligned}$$

$\delta\omega \equiv \delta\omega^L + \delta\omega^{NL}$ with $\delta\omega^L \equiv [\omega_1 + \omega_3 - 2\omega_2]$ and $\delta\omega^{NL} \equiv [\omega_1^{NL} + \omega_3^{NL} - 2\omega_2^{NL}]$, where
 $\omega_k^{NL} = \lambda'_k + \nu'_{k1} r_1^2 + \nu'_{k2} r_2^2 + \nu'_{k3} r_3^2$.

Periodic solution

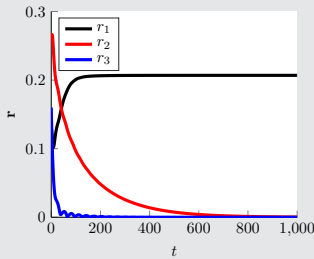


Modelling of the interaction

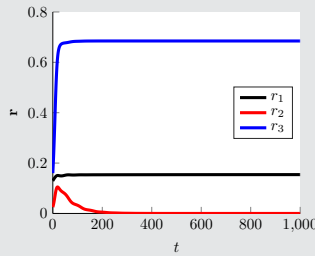
$$\begin{aligned}\dot{r}_j &= r_j [\lambda_j + \sum_k^N \operatorname{Re}(\nu_{jk}) r_k^2] + f_{r_j}(r, \phi) \\ \dot{\psi} &= \delta\omega + f_\psi(r, \phi)\end{aligned}$$

$\delta\omega \equiv \delta\omega^L + \delta\omega^{NL}$ with $\delta\omega^L \equiv [\omega_1 + \omega_3 - 2\omega_2]$ and $\delta\omega^{NL} \equiv [\omega_1^{NL} + \omega_3^{NL} - 2\omega_2^{NL}]$, where
 $\omega_k^{NL} = \lambda'_k + \nu'_{k1} r_1^2 + \nu'_{k2} r_2^2 + \nu'_{k3} r_3^2$.

Periodic solution



Quasiperiodic solution

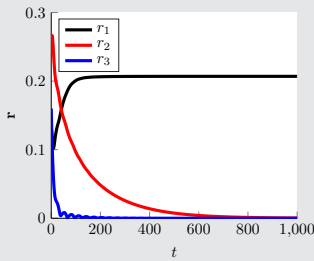


Modelling of the interaction

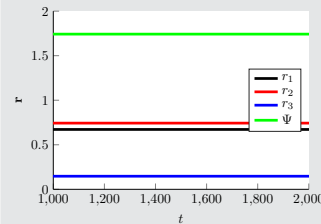
$$\begin{aligned}\dot{r}_j &= r_j [\lambda_j + \sum_k^N \operatorname{Re}(\nu_{jk}) r_k^2] + f_{r_j}(r, \phi) \\ \dot{\Psi} &= \delta\omega + f_{\Psi}(r, \phi)\end{aligned}$$

$\delta\omega \equiv \delta\omega^L + \delta\omega^{NL}$ with $\delta\omega^L \equiv [\omega_1 + \omega_3 - 2\omega_2]$ and $\delta\omega^{NL} \equiv [\omega_1^{NL} + \omega_3^{NL} - 2\omega_2^{NL}]$, where
 $\omega_k^{NL} = \lambda'_k + \nu'_{k1} r_1^2 + \nu'_{k2} r_2^2 + \nu'_{k3} r_3^2$.

Periodic solution



\mathbb{T}^2 sol. (phase-locked)

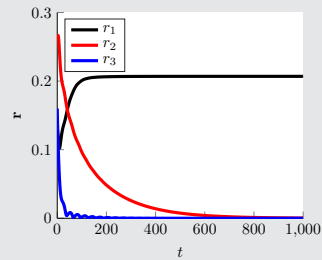


Modelling of the interaction

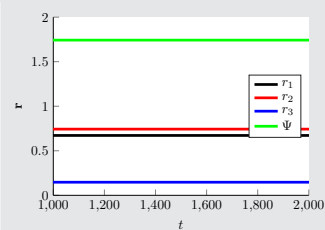
$$\begin{aligned}\dot{r}_j &= r_j [\lambda_j + \sum_k^N \operatorname{Re}(\nu_{jk}) r_k^2] + f_{r_j}(r, \phi) \\ \dot{\Psi} &= \delta\omega + f_{\Psi}(r, \phi)\end{aligned}$$

$\delta\omega \equiv \delta\omega^L + \delta\omega^{NL}$ with $\delta\omega^L \equiv [\omega_1 + \omega_3 - 2\omega_2]$ and $\delta\omega^{NL} \equiv [\omega_1^{NL} + \omega_3^{NL} - 2\omega_2^{NL}]$, where
 $\omega_k^{NL} = \lambda'_k + \nu'_{k1} r_1^2 + \nu'_{k2} r_2^2 + \nu'_{k3} r_3^2$.

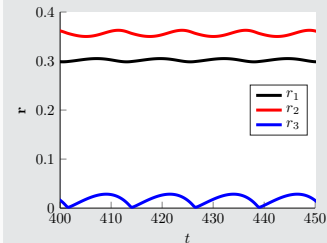
Periodic solution



\mathbb{T}^2 sol. (phase-locked)



Modulated solution



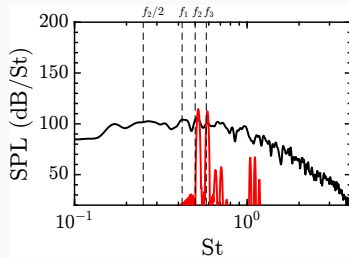
Broadband-tonal sound in subsonic rounded impinging jet (III)

Modelling of the interaction

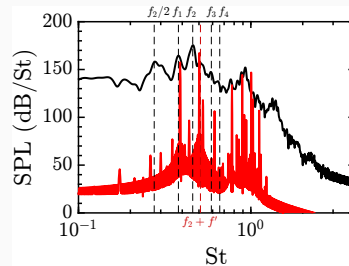
$$\begin{aligned}\dot{r}_j &= r_j [\lambda_j + \sum_k^N \text{Re}(\nu_{jk}) r_k^2] + f_{rj}(\mathbf{r}, \phi) \\ \dot{\psi} &= \delta\omega + f_\psi(\mathbf{r}, \phi)\end{aligned}$$

$\delta\omega \equiv \delta\omega^L + \delta\omega^{NL}$ with $\delta\omega^L \equiv [\omega_1 + \omega_3 - 2\omega_2]$ and $\delta\omega^{NL} \equiv [\omega_1^{NL} + \omega_3^{NL} - 2\omega_2^{NL}]$, where
 $\omega_k^{NL} = \lambda'_k + \nu'_{k1} r_1^2 + \nu'_{k2} r_2^2 + \nu'_{k3} r_3^2$.

$M_J \approx 0.35, Re = 2000$



$M_J \approx 0.7, Re = 2000$



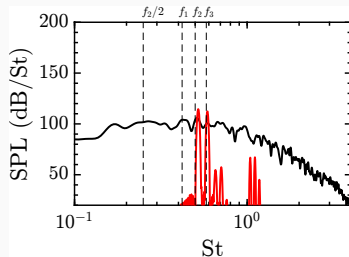
Broadband-tonal sound in subsonic rounded impinging jet (III)

Modelling of the interaction

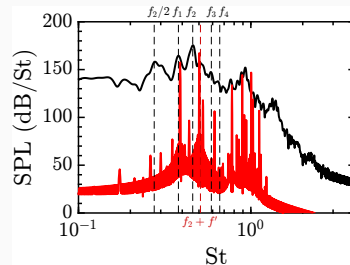
$$\begin{aligned}\dot{r}_j &= r_j \left[\lambda_j + \sum_k^N \operatorname{Re}(\nu_{jk}) r_k^2 \right] + f_{rj}(\mathbf{r}, \phi) \\ \dot{\Psi} &= \delta\omega + f_\Psi(\mathbf{r}, \phi)\end{aligned}$$

$\delta\omega \equiv \delta\omega^L + \delta\omega^{NL}$ with $\delta\omega^L \equiv [\omega_1 + \omega_3 - 2\omega_2]$ and $\delta\omega^{NL} \equiv [\omega_1^{NL} + \omega_3^{NL} - 2\omega_2^{NL}]$, where
 $\omega_k^{NL} = \lambda'_k + \nu'_{k1} r_1^2 + \nu'_{k2} r_2^2 + \nu'_{k3} r_3^2$.

$M_J \approx 0.35, Re = 2000$



$M_J \approx 0.7, Re = 2000$

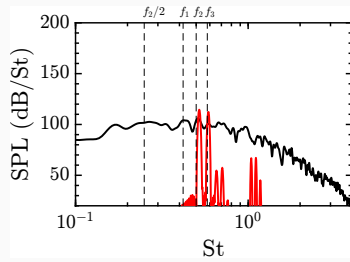


The "peaks" are of the same order of magnitude but the rest... Reasonable reconstruction of the peaks.

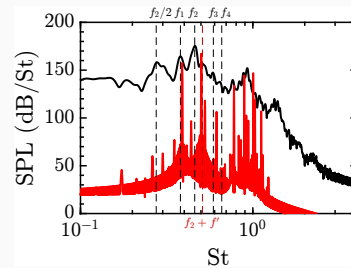
Issues with the modelling

- At low Mach numbers, the (DNS) spectrum is broadband, but the normal form reconstruction is *tonal*. \Rightarrow Model the equi-distant frequency "imperfection" by an stochastic term
 $\delta\omega^{NL} \mapsto \delta\omega^{NL}(1 + dW)$
- It does not characterise the frequency associated with the period doubling bifurcation ($f_2/2$).

$M_J \approx 0.35, Re = 2000$



$M_J \approx 0.7, Re = 2000$

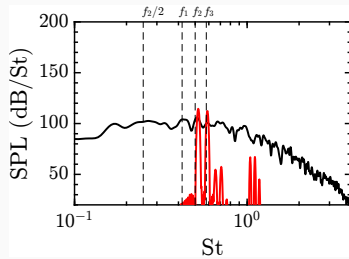


Broadband-tonal sound in subsonic rounded impinging jet (III)

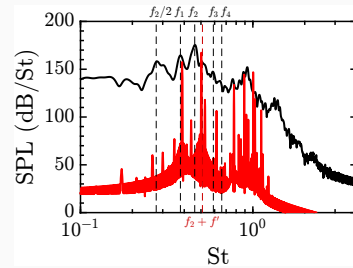
Issues with the modelling

- At low Mach numbers, the (DNS) spectrum is broadband, but the normal form reconstruction is *tonal*. \Rightarrow Model the equi-distant frequency "imperfection" by an stochastic term
 $\delta\omega^{NL} \mapsto \delta\omega^{NL}(1 + dW)$
- It does not characterise the frequency associated with the period doubling bifurcation ($f_2/2$). It is a secondary instability, here we do not treat it.

$M_J \approx 0.35, Re = 2000$



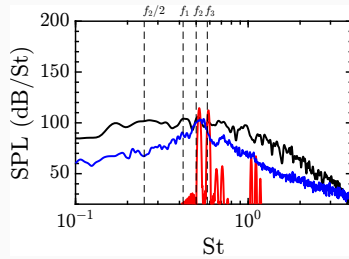
$M_J \approx 0.7, Re = 2000$



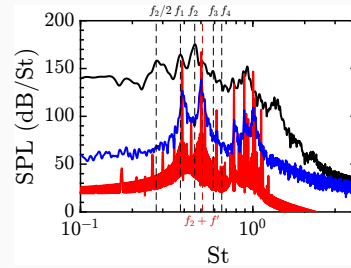
Stochastic modelling

- Justifications for $\delta\omega^{NL} \mapsto \delta\omega^{NL}(1 + dW)$ in the resonant phase equation:
 - a) It accounts for the frequency shift from cycle to cycle of the feedback mechanism due to changes of position and magnitude of the vortical sources of sound in the radial shear layer, and thus affecting the closure of the feedback loop.
 - b) It is assumed to account for the frequency shift of the feedback mechanism underpinning the instability caused by the vortices convected to the nozzle lip.

$M_J \approx 0.35, Re = 2000$



$M_J \approx 0.7, Re = 2000$



Mode interaction

- Analysis of a variety of scenarios displaying codimension-two bifurcations \implies
 - **Methodology**
 - Data assimilation and optimisation techniques.⁵
 - Stochastic centre manifold (coarse-grained) reduction for systems far from equilibrium.^{6,7}
 - **Application to configurations with moving interfaces**
 - Rising bubble or falling rigid objects.
 - Fluid-Structure Interaction.

Most codes are available in, otherwise feel free to ask us!

<https://gitlab.com/stabfem/StabFem>

⁵Cenedese et al., "Data-driven modeling and prediction of non-linearizable dynamics via spectral submanifolds".

⁶Wouters et al., "Edgeworth expansions for slow-fast systems and their application to model reduction for finite time scale separation".

⁷Schmuck et al., "New stochastic mode reduction strategy for dissipative systems".

Questions

1. J. Sierra, D. Fabre, E. Knobloch. A Note on the steady-state mode and Hopf mode interaction in the presence of O(2)-symmetry. *Physical Review E (submitted)*
2. A. Corrochano, J. Sierra, J.A. Martin, S. Le Clainche, D. Fabre. Mode selection in concentric jets with resonance 1:2 *Journal of Fluid Mechanics (under review)*
3. J. Sierra, F. Giannetti, D. Fabre On the linear and nonlinear mechanisms for the tonal and broadband noise of subsonic rounded impinging jet. *Journal of Fluid Mechanics (submitted)*
4. L. Hirschberg, J. I. Guzman, A. Morgans, J. Sierra, D. Fabre, A. Hirschberg. Linear Theory and Experiments for Laminar Bias Flow Impedance. *AIAA to be submitted*.
5. J. Sierra, V. Citro, D. Fabre, F. Giannetti. Bifurcation scenario in the two-dimensional laminar flow past a rotating cylinder. *Journal of Fluid Mechanics 905*.
6. J. Sierra, M. Lorite, J.I. Jimenez, V.Citro, D Fabre. Unveiling the competitive role of global modes in the pattern formation of rotating sphere flows. *Journal of Fluid Mechanics 942*.
7. J. Sierra, P. Jolivet, V. Citro, F. Giannetti. Adjoint-based sensitivity analysis of periodic orbits by the Fourier–Galerkin method *Journal of Computational Physics 440*
8. J. Sierra, V. Citro, D. Fabre, F. Giannetti. Efficient computation of time-periodic compressible flows with spectral techniques *Computer Methods in Applied Mechanics and Engineering 393*.
9. J. Sierra, P. Bonnefis, A. Tirri, D. Fabre, J. Magnaudet. Dynamics of a gas bubble in a straining flow: deformation, oscillations, self-propulsion. *Physical Review Fluids, 7(11), 113603*.
10. A. Tirri, A. Nitti, J. Sierra, F. Giannetti, M. D. de Tullio. Linear stability analysis of fluid–structure interaction problems with an immersed boundary method. *Journal of Fluids and Structures, 117, 103830*
11. J. Sierra, V. Citro, D. Fabre Efficient stability analysis of fluid flows using complex mapping techniques. *Computer Physics Communications 251*.
12. J. Sierra, V. Citro, D. Fabre, F. Giannetti. Acoustic instability prediction of the flow through a circular aperture in a thick plate via an impedance criterion. *Journal of Fluid Mechanics 943*.
13. J. Sierra, V. Citro F. Giannetti Optimal explicit Runge-Kutta methods for compressible Navier-Stokes equations. *Applied Numerical Mathematics*.
14. G. Saez, J. Sierra, J. Gressier. Spectral Difference Raviart–Thomas Method for Two and Three-Dimensional Elements and Its Connection with the Flux Reconstruction Formulation. *Journal of Scientific Computing*.
15. G. Saez, J. Sierra, G. Grondin, J. Gressier. On the properties of high-order least-squares finite-volume schemes. *Journal of Computational Physics*

The linearised equations are

$$\left(-i\omega \mathbf{B}|_{q_0} + \mathbf{D}\mathbf{F}|_{q_0} \right) \hat{\mathbf{q}} = 0, \text{ with } \mathbf{B}|_{q_0} = \text{diag}(1, \rho_0 \mathbf{I}, \rho_0 T_0, 0, 0), \quad (11)$$

$$\mathbf{u}_0 \cdot \nabla \hat{p} + \hat{p} \nabla \cdot \mathbf{u}_0 + \hat{\mathbf{u}} \cdot \nabla \rho_0 + \rho_0 \nabla \cdot \hat{\mathbf{u}} \quad (12a)$$

$$\hat{p} \mathbf{u}_0 \cdot \nabla \mathbf{u}_0 + \rho_0 \mathbf{u}_0 \cdot \nabla \hat{\mathbf{u}} + \rho_0 \hat{\mathbf{u}} \cdot \nabla \mathbf{u}_0 + \nabla \hat{p} - \frac{1}{Re} \nabla \cdot \tau(\hat{\mathbf{u}}) \quad (12b)$$

$$\mathbf{D}\mathbf{F}|_{q_0} \hat{\mathbf{q}} = \begin{cases} \mathbf{u}_0 \cdot \nabla \hat{p} + \hat{p} \nabla \cdot \mathbf{u}_0 + \hat{\mathbf{u}} \cdot \nabla \rho_0 + \rho_0 \nabla \cdot \hat{\mathbf{u}} & (12a) \\ \hat{p} \mathbf{u}_0 \cdot \nabla \mathbf{u}_0 + \rho_0 \mathbf{u}_0 \cdot \nabla \hat{\mathbf{u}} + \rho_0 \hat{\mathbf{u}} \cdot \nabla \mathbf{u}_0 + \nabla \hat{p} - \frac{1}{Re} \nabla \cdot \tau(\hat{\mathbf{u}}) & (12b) \\ -\gamma(\gamma-1) \frac{M_\infty^2}{Re} (\tau(\hat{\mathbf{u}}) : \mathbf{D}(\mathbf{u}_0) + \tau(\mathbf{u}_0) : \mathbf{D}(\hat{\mathbf{u}})) - \frac{\gamma}{Pr Re} \Delta \hat{T} \\ + \rho_0 T_0 \mathbf{u}_0 \cdot \nabla \hat{s} + \rho_0 T_0 \hat{\mathbf{u}} \cdot \nabla s_0 + \hat{p} T_0 \mathbf{u}_0 \cdot \nabla s_0 + \rho_0 \hat{T} \mathbf{u}_0 \cdot \nabla s_0 & (12c) \\ \rho_0 T_0 \hat{s} + (\gamma-1) T_0 \hat{p} - \rho_0 \hat{T} & (12d) \\ -\rho_0 \hat{T} - \hat{p} T_0 + \gamma M_\infty^2 \hat{p} & (12e) \end{cases}$$

And their adjoint counterpart are

$$\left(i\bar{\omega} \mathbf{B}|_{q_0} + \mathbf{D}\mathbf{F}^\dagger|_{q_0} \right) \hat{\mathbf{q}}^\dagger = 0, \text{ with } \mathbf{B}|_{q_0} = \text{diag}(1, \rho_0 \mathbf{I}, \rho_0 T_0, 0, 0), \quad (13)$$

$$\mathbf{D}\mathbf{F}^\dagger|_{q_0} \hat{\mathbf{q}}^\dagger = \begin{cases} -\mathbf{u}_0 \cdot \nabla \hat{\rho}^\dagger + (\mathbf{u}_0 \cdot \nabla \mathbf{u}_0) \cdot \hat{\mathbf{u}}^\dagger \\ + (\mathbf{u}_0 \cdot \nabla s_0) \hat{s}^\dagger + T_0 ((\gamma - 1) \hat{T}^\dagger - \hat{\rho}^\dagger) \end{cases} \quad (14a)$$

$$\begin{cases} -\rho_0 \mathbf{u}_0 \cdot \nabla \hat{\mathbf{u}}^\dagger + \rho_0 \hat{\mathbf{u}}^\dagger \cdot (\nabla \mathbf{u}_0)^T - \frac{1}{\text{Re}} \nabla \cdot \tau(\hat{\mathbf{u}}^\dagger) \\ -\rho_0 \nabla \hat{\rho}^\dagger + 2\gamma(\gamma - 1) \frac{M_\infty^2}{\text{Re}} \nabla \cdot (\hat{s}^\dagger \tau(\mathbf{u}_0)) + \rho_0 T_0 \hat{s}^\dagger \nabla s_0 \end{cases} \quad (14b)$$

$$\begin{cases} -\rho_0 T_0 \mathbf{u}_0 \cdot \nabla \hat{s}^\dagger + \rho_0 T_0 \hat{T}^\dagger \\ \rho_0 T_0 \hat{s}^\dagger \mathbf{u}_0 \cdot \nabla s_0 - \frac{\gamma}{\text{Pr Re}} \nabla^2 \hat{s}^\dagger - \rho_0 \hat{\rho}^\dagger - \rho_0 \hat{T}^\dagger \end{cases} \quad (14c)$$

$$\begin{cases} \gamma M_\infty^2 \hat{\rho}^\dagger - \nabla \cdot \hat{\mathbf{u}}^\dagger \end{cases} \quad (14d)$$

$$(14e)$$

The pressure decomposition is derived from the linearised momentum equation. Considering an isenstropic relationship between density and pressure fluctuations, i.e, $\hat{\rho}T_0 = M_\infty^2 \hat{p}$, and taking divergence of the linearised momentum equation, we end up with the following elliptic equation for the pressure,

$$-\frac{1}{\rho_0} \Delta \hat{p} + \frac{\nabla \rho_0 \cdot \nabla \hat{p}}{\rho_0^2} - \nabla \cdot \left(\frac{M_\infty^2}{T_0} (\mathbf{u}_0 \cdot \nabla \mathbf{u}_0) \frac{\hat{p}}{\rho_0} \right) = \nabla \cdot (\mathbf{u}_0 \cdot \nabla \hat{\mathbf{u}}) + \nabla \cdot (\hat{\mathbf{u}} \cdot \nabla \mathbf{u}_0) + i\omega \nabla \cdot \hat{\mathbf{u}} - \frac{1}{Re} \nabla \cdot (\nabla \cdot \tau(\hat{\mathbf{u}})).$$

Decomposing the velocity field into acoustic and hydrodynamic and leaving the viscous dissipation term to the entropic component, we end up with the following decomposition of the pressure,

Temperature and density decomposition

$$-\frac{1}{\rho_0} \Delta \hat{\rho}_{\text{ac}} + \frac{\nabla \rho_0 \cdot \nabla \hat{\rho}_{\text{ac}}}{\rho_0^2} - \nabla \cdot \left(\frac{M_\infty^2}{T_0} (\mathbf{u}_0 \cdot \nabla \mathbf{u}_0) \frac{\hat{\rho}_{\text{ac}}}{\rho_0} \right) = i\omega \nabla \cdot \hat{\mathbf{u}}_{\text{ac}} + \nabla \cdot (\mathbf{u}_0 \cdot \nabla \hat{\mathbf{u}}_{\text{ac}}) + \nabla \cdot (\hat{\mathbf{u}}_{\text{ac}} \cdot \nabla \mathbf{u}_0) \quad (15a)$$

$$-\frac{1}{\rho_0} \Delta \hat{\rho}_{\text{hyd}} + \frac{\nabla \rho_0 \cdot \nabla \hat{\rho}_{\text{hyd}}}{\rho_0^2} - \nabla \cdot \left(\frac{M_\infty^2}{T_0} (\mathbf{u}_0 \cdot \nabla \mathbf{u}_0) \frac{\hat{\rho}_{\text{hyd}}}{\rho_0} \right) = \nabla \cdot (\mathbf{u}_0 \cdot \nabla \hat{\mathbf{u}}_{\text{hyd}}) + \nabla \cdot (\hat{\mathbf{u}}_{\text{hyd}} \cdot \nabla \mathbf{u}_0) \quad (15b)$$

$$\hat{\rho}_s = \hat{\rho} - \hat{\rho}_{\text{hyd}} - \hat{\rho}_{\text{ac}}. \quad (15c)$$

$$\hat{T}_{\text{ac}} = (\gamma - 1) M_\infty^2 \hat{\rho}_{\text{ac}}, \quad \hat{T}_{\text{hyd}} = (\gamma - 1) M_\infty^2 \hat{\rho}_{\text{hyd}}, \quad \hat{T}_s = \hat{T} - \hat{T}_{\text{ac}} - \hat{T}_{\text{hyd}}, \quad (16)$$

$$\hat{\rho}_{\text{ac}} = M_\infty^2 \frac{\rho_0}{T_0} \hat{\rho}_{\text{ac}}, \quad \hat{\rho}_{\text{hyd}} = M_\infty^2 \frac{\rho_0}{T_0} \hat{\rho}_{\text{hyd}}, \quad \hat{\rho}_s = \hat{\rho} - \hat{\rho}_{\text{ac}} - \hat{\rho}_{\text{hyd}}. \quad (17)$$

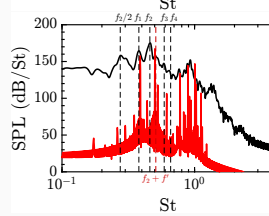
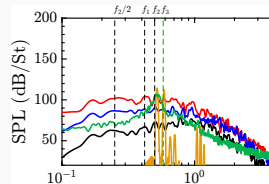
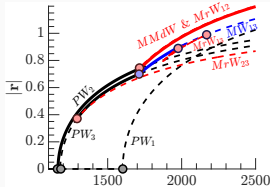
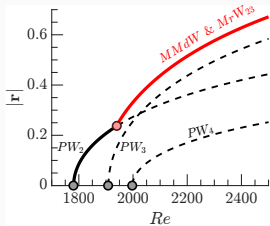
Adjoint decomposition

Overall, the adjoint is decomposed as follows,

$$\begin{aligned}\hat{\mathbf{u}}^\dagger &= \hat{\mathbf{u}}_{\text{hyd}}^\dagger + \hat{\mathbf{u}}_{\text{ac}}^\dagger = \nabla \phi_c^\dagger + \nabla \times \Psi^\dagger \\ \hat{s}^\dagger &= \hat{s}_s^\dagger \\ \hat{\rho}^\dagger &= \hat{\rho}_{\text{ac}}^\dagger + \hat{\rho}_{\text{hyd}}^\dagger + \hat{\rho}_s^\dagger \\ \hat{p}^\dagger &= \hat{p}_{\text{ac}}^\dagger = \frac{\nabla \cdot \hat{\mathbf{u}}^\dagger}{\gamma M_\infty^2} \\ \hat{T}^\dagger &= \hat{T}_{\text{ac}}^\dagger + \hat{T}_s^\dagger = -\frac{\nabla \cdot \hat{\mathbf{u}}^\dagger}{\gamma M_\infty^2} + \left(\hat{s}^\dagger \mathbf{u}_0 \cdot \nabla s_0 - \frac{\gamma}{\text{Pr Re}} \frac{1}{\rho_0} \Delta s_0 \right)\end{aligned}$$

Broadband-tonal sound in subsonic rounded impinging jet (backup)

$$\begin{aligned}
 \dot{r}_1 &= r_1 [\lambda_1^R + \nu_{11}^R r_1^2 + \nu_{12}^R r_2^2 + \nu_{13}^R r_3^2] + r_2^2 r_3 [\cos(\psi) \chi_1^R + \sin(\psi) \chi_1^I] \\
 \dot{r}_2 &= r_2 [\lambda_2^R + \nu_{21}^R r_1^2 + \nu_{22}^R r_2^2 + \nu_{23}^R r_3^2] + r_1 r_2 r_3 [\cos(\psi) \chi_2^R - \sin(\psi) \chi_2^I] \\
 \dot{r}_3 &= r_3 [\lambda_3^R + \nu_{31}^R r_1^2 + \nu_{32}^R r_2^2 + \nu_{33}^R r_3^2] + r_2^2 r_1 [\cos(\psi) \chi_3^R + \sin(\psi) \chi_3^I] \\
 \dot{\psi} &= \delta\omega + \cos(\psi) [-\chi_3^I r_1 r_2^2 / r_3 + 2\chi_2^I r_1 r_3 - \chi_1^I r_2 r_3^2 / r_1] \\
 &\quad - \sin(\psi) [\chi_3^R r_1 r_2^2 / r_3 + 2\chi_2^R r_1 r_3 + \chi_1^R r_2 r_3^2 / r_1].
 \end{aligned}$$



Pressure closure of the loop from outside

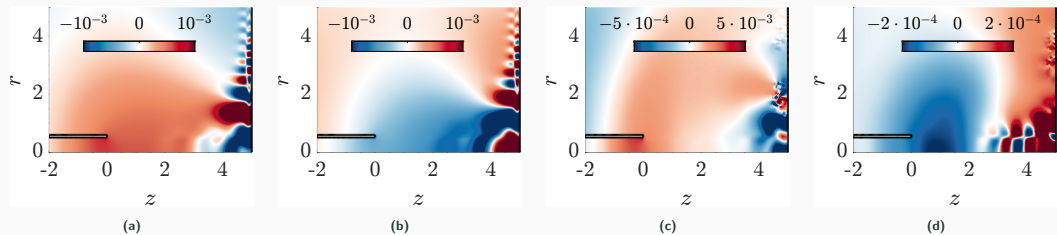


Figure 2: (a,b) Real and imaginary part of the pressure of mode (b) at $M_\infty = 0.2$. (c,d) Pressure fluctuations issued from an axisymmetric time-stepping simulation at $M_\infty = 0.2$ and $Re = 2200$.

Normal form (polar form)

However, it is more convenient to work with the normal form in its polar form ($a_j = r_j e^{i\phi_j}$) for $j = 0, 1, 2$, and the phase $\Psi = \phi_1 - \phi_2 - 2\phi_0$

$$\begin{aligned}\dot{r}_0 &= [\lambda_s + l_0 r_0^2 + l_1(r_1^2 + r_2^2)] r_0 \\ &\quad + l_3 r_0 r_1 r_2 \cos \Psi\end{aligned}$$

$$\begin{aligned}\dot{r}_1 &= [\lambda_h + B_r r_1^2 + (A_r + B_r) r_2^2 + C_r r_0^2] r_1 \\ &\quad + r_0^2 r_2 (D_r \cos \Psi + D_i \sin \Psi)\end{aligned}$$

$$\begin{aligned}\dot{r}_2 &= [\lambda_h + B_r r_2^2 + (A_r + B_r) r_1^2 + C_r r_0^2] r_2 \\ &\quad + r_0^2 r_1 (D_r \cos \Psi - D_i \sin \Psi)\end{aligned}$$

$$\begin{aligned}\dot{\Psi} &= (A_i - 2l_2)(r_2^2 - r_1^2) - 2l_3 r_1 r_2 \sin \Psi \\ &\quad + r_0^2 D_i \cos \Psi \left[\frac{r_2}{r_1} - \frac{r_1}{r_2} \right] - r_0^2 D_r \sin \Psi \left[\frac{r_2}{r_1} + \frac{r_1}{r_2} \right]\end{aligned}$$

which allows us to reduce dynamics to a four dimensional subspace (slicing the two continuous symmetries, now discrete).

Normal form reduction (Order 2)

Non-linear second order terms in ε are

$$\begin{aligned}\mathbf{F}_{(\varepsilon^2)} &\equiv \sum_{j,k=0}^2 \left(a_j a_k \mathbf{N}(\hat{\mathbf{q}}_j, \hat{\mathbf{q}}_k) e^{-i(m_j+m_k)\theta} e^{-i(\omega_j+\omega_k)t} + \text{c.c.} \right) \\ &+ \sum_{j,k=0}^2 \left(a_j \bar{a}_k \mathbf{N}(\hat{\mathbf{q}}_j, \bar{\hat{\mathbf{q}}}_k) e^{-i(m_j-m_k)\theta} e^{-i(\omega_j-\omega_k)t} + \text{c.c.} \right) \\ &+ \sum_{\ell=0}^2 \eta_\ell \mathbf{G}(\mathbf{Q}_0, \mathbf{e}_\ell),\end{aligned}$$

The second order term can be expanded as follows

$$\mathbf{q}_{(\varepsilon^2)} \equiv \sum_{\substack{j,k=0 \\ k \leq j}}^2 (a_j a_k \hat{\mathbf{q}}_{j,k} + a_j \bar{a}_k \hat{\mathbf{q}}_{j,-k} + \text{c.c.}) + \sum_{\ell=0}^2 \eta_\ell \mathbf{Q}_0^{(\eta_\ell)}, \quad (19)$$

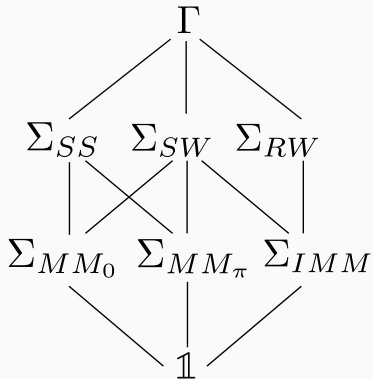
Finally, second-order terms are computed by solving

$$\begin{aligned}\mathbf{J}_{(\omega_j+\omega_k, m_j+m_k)} \hat{\mathbf{q}}_{j,k} &= \hat{\mathbf{F}}_{(\varepsilon^2)}^{(j,k)}, \\ \mathbf{J}_{(0,0)} \mathbf{Q}_0^{(\eta_\ell)} &= \mathbf{G}(\mathbf{Q}_0, \mathbf{e}_\ell).\end{aligned}$$

Isotropy lattice – Primary bifurcations

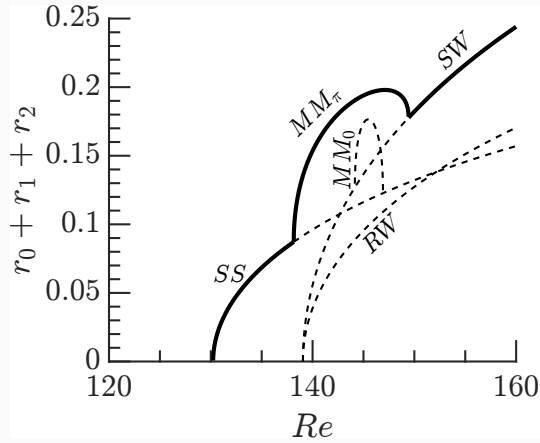
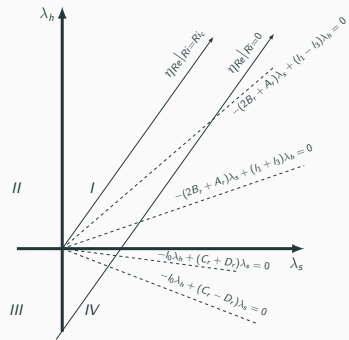
Name	Representative	Iso. group (complex)	Iso. group (polar)	Frequencies
Pure modes:				
TS	$(0, 0, 0, nd)$	$O(2) \times S^1$	$D_4 \rtimes \mathbb{Z}_2(\kappa)$	0
SS	$(r_a, 0, 0, nd)$	$\mathbb{Z}_2(\kappa) \times S^1$	$\mathbb{Z}_2(\kappa) \times \mathbb{Z}_2(\Phi_\pi)$	0
RW	$(0, r_a, 0, nd)$	$\widetilde{SO(2)}$	$\mathbb{Z}_4(R_{\pi/2}\Phi_{\pi/2})$	1
SW	$(0, r_a, r_a, nd)$	$\mathbb{Z}_2(\kappa) \times \mathbb{Z}_2(R_\pi\Phi_\pi)$	$\mathbb{Z}_2(\kappa) \times \mathbb{Z}_2(R_\pi\Phi_\pi)$	1
Mixed modes:				
MM_0	$(r_a, r_b, r_b, 0)$	$\mathbb{Z}_2(\kappa)$	$\mathbb{Z}_2(\kappa)$	1
MM_π	(r_a, r_b, r_b, π)	$\mathbb{Z}_2(\kappa \cdot R_\pi\Phi_\pi)$	$\mathbb{Z}_2(\kappa \cdot R_\pi\Phi_\pi)$	1
IMM	$(0, r_a, r_b, \Psi)$	$\mathbb{Z}_2(R_\pi\Phi_\pi)$	$\mathbb{Z}_2(R_\pi\Phi_\pi)$	1
Precessing waves:				
General	(r_a, r_b, r_c, Ψ)	$\mathbb{1}$	$\mathbb{1}$	2
Type A	(r_a, r_b, r_b, Ψ)	$\mathbb{1}$	$\mathbb{1}$	2
Type B	$(r_a, r_b, r_c, 0 \text{ or } \pi)$	$\mathbb{1}$	$\mathbb{1}$	2
Type C	$(r_a, r_b, 0, \Psi)$	$\mathbb{1}$	$\mathbb{1}$	2

Nomenclature in different problems



Name	Name (TC)	Name (WFA)
TS	Taylor Couette Flow	Axisymmetric state
SS	Taylor Vortex Flow	Steady shedding
SW	Ribbon cells	Standing wave
RW	Spiral vortex	Spiral Shedding state
MM_0	Twisted vortices	Reflection Symmetry Preserving
MM_π	Wavy vortices	Reflection Symmetry Breaking
IMM	Wavy Spirals	(-)
PrW	(-)	(-)

Construction of the bifurcation diagram

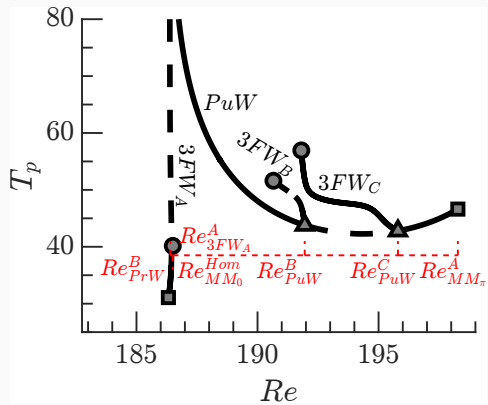
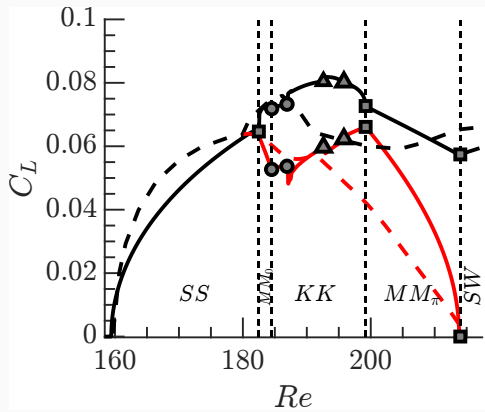


Modulated bifurcations

Name	Representative	Isotropy group	Frequencies
$\widetilde{MM}_{0,\pi}$	$(r_a(t), r_b(t), r_b(t), 0 \text{ or } \pi)$	$\mathbb{1}$	2
\widetilde{IMM}	$(0, r_b, r_c, \Psi(t))$	$\mathbb{1}$	2
PuW	$(r_a(t), r_b(t), r_c(t), \Psi(t))$ with $\bar{r}_b = \bar{r}_c$ and $\overline{\sin \Psi} = 0$	$\mathbb{1}$	2
3-frequency waves: (3FW)			
General	$(r_a(t), r_b(t), r_c(t), \Psi(t))$	$\mathbb{1}$	3
Type A	$(r_a(t), r_b(t), r_b(t), \Psi(t))$ with $\overline{\sin \Psi} \neq 0$	$\mathbb{1}$	3
Type B	$(r_a(t), r_b(t), r_c(t), 0 \text{ or } \pi)$ with $\bar{r}_b \neq \bar{r}_c$	$\mathbb{1}$	3
Type C	$(0, r_b(t), r_c(t), \text{nd})$ with $\bar{r}_b \neq \bar{r}_c$	$\mathbb{1}$	3
Type D	$(r_a(t), r_b(t), 0, \Psi(t))$ with $\overline{\sin \Psi} \neq 0$	$\mathbb{1}$	3

The quasiperiodic state $\widetilde{MM}_{0,\pi}$ is known as Modulated Wavy Vortex Flow (MWVF) in the Taylor

A more complex bifurcation diagram



Robust (asymptotically stable) heteroclinic cycles

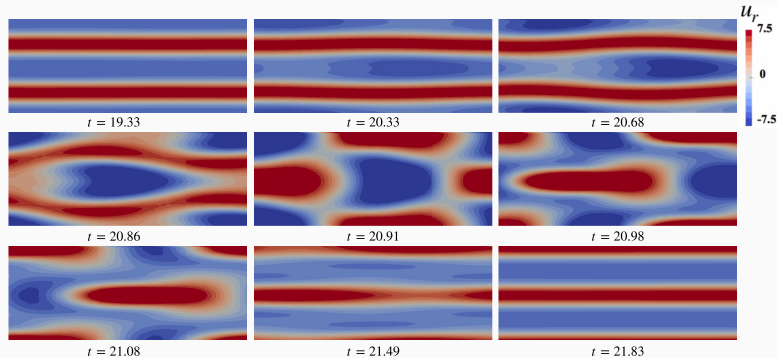
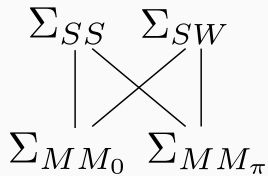


Figure 3: Courtesy of [bengana2019spirals](#). Identified in the region of Wavy Spirals (IMM), near the boundary of Modulated Wavy Vortex ($\widetilde{MM}_{0,\pi}$). The physical mechanism is [SSP dessup2018self](#)